Stony Brook University

Diagenetic behavior of structural materials formed by benthic macrofauna

A Thesis Presented

by

Aleya Kaushik

to

The Graduate School

in Partial Fulfillment of the

Requirements

for the Degree of

Master of Science

in

Marine and Atmospheric Science

Stony Brook University

August 2011

Stony Brook University

The Graduate School

Aleya Kaushik

We, the thesis committee for the above candidate for the

Master of Science degree, hereby recommend

acceptance of this thesis.

Robert C. Aller – Thesis Advisor
Distinguished Professor
School of Marine & Atmospheric Sciences

Cindy Lee
Distinguished Professor
School of Marine & Atmospheric Sciences

Qingzhi Zhu
Assistant Professor
School of Marine & Atmospheric Sciences

Josephine Y. Aller
Research Professor
School of Marine & Atmospheric Sciences

This thesis is accepted by the Graduate School

Lawrence Martin
Dean of the Graduate School

Abstract of the Thesis

Diagenetic behavior of structural materials formed by benthic macrofauna

by

Aleya Kaushik

Master of Science

in

Marine and Atmospheric Science

Stony Brook University

2011

The role of biogenic tube material produced by polychaete worms in the cycling of organic matter in marine sediments is relatively unknown. Here I characterize the fate of the constructional material of one polychaete, *Chaetopterus variopedatus*. Preliminary experiments showed little to no degradation under oxygenated conditions or in anoxic seawater, so degradation was followed in anoxic sediment. SEM studies revealed distinct morphological changes during anoxic decomposition. The tube walls are made from a well-formed cross-woven mesh of fibers, which are individually typically 100 nm in diameter. In incubated tubes, the integrity of this mesh structure is lost during decomposition. SEM and X-ray studies of tube material also revealed the presence of swathes of manganese micro-nodular structures in fresh tubes that are also lost during anoxic decomposition.

The time-scale of organic matter release from these tubes is on the order of months, with a higher pulse release of organic matter in the first 60 days, followed by a more gradual release. In addition to the slow release of organic matter, the tube material also acts as a sink for redox-sensitive metals including manganese and iron. Manganese is typically 40X enriched compared to surrounding sediments, whereas the iron is typically 2.5X enriched. Manganese is lost more rapidly and continuously from the tubes over time compared to iron, which after an initial decrease stays fairly constant. The time-scale of release of manganese is on the order of weeks, with >50% being lost within the first month. This has significant effects on the concentration of manganese in surrounding sediments and porewater.

In localized areas where they are found, *C. variopedatus* tube production can account for ~12% of the average annual POC flux to the benthos from water column primary production, ~11% of the PON flux and >100% of the POP flux to the benthos.

Table of Contents

List of Figures

Figure:

List of Tables

I. INTRODUCTION

Marine sediments can be viewed as a complex mix of physical, biological and chemical microenvironments. The bulk properties of any given sediment will be determined by the properties and interactions within such microenvironments. Macrofauna can have profound effects on organic matter decomposition and remineralization in sediments (Aller, 1982, 1988 & 2001; Table 1). Many studies have shown that benthic animals generally stimulate transport and reaction rates in bioturbated sediments relative to sediments with less infauna (e.g., Aller & Yingst, 1985, Aller, 1994). Benthic animals affect the distribution of particles and fluids by: (a) translocating material between different reaction zones during the processes of feeding, burrowing and tube construction, (b) altering reaction and solute diffusion geometries by burrow and fecal pellet formation, creating a variety of variably oriented microenvironments rather than a vertically stratified distribution, as would generally be observed in non-bioturbated sediments with stable depositional regimes, (c) influencing the distribution of microbial populations that mediate reactions through physical and chemical reworking of the sediment, (d) creating new organic substrates such as mucus secretions and similar tube constructional materials which are introduced into the deposit independent of physical sedimentation processes.

Particulate organic matter deposited in sediments can be remineralized, altered, recycled and buried. Despite the complex composition of organic matter, and the variety of complex multi-step mechanisms for organic matter remineralization, the equations used to model net remineralization processes are often quite simple. The most often used approach is the *multi-G model* (Jorgensen, 1978, Berner, 1981), which assumes that sediment organic matter is composed of various groups, or fractions of organic matter (G_i) that have different degrees of reactivity and that the sum of these individual fractions (G) then comprises the total amount of organic matter in sediments. Assuming that each individual component undergoes first-order decomposition, the overall rate of decomposition is then expressed by:

$$dG/dt = -\sum k_i G_i \qquad (1)$$

where the degree of reactivity is given by k. In any given sediment, a common assumption is that there are three primary organic matter fractions: two that undergo remineralization at different rates depending on their reactivity and one that is inert on the time scale of the particular system and represents the asymptotic background level of organic matter observed (Soetaert, 1996, Boudreau, 1997). The “reactive” fraction undergoes remineralization on depth scales from < 1 cm in the deep sea to 10-20 cm in continental margin and coastal sediments, whereas the less reactive component decomposes on longer depth scales, from several centimeters in the deep sea to ~ 1 m in shallow sediments.

Work by Burdige (1991) demonstrated that the “reactive” organic matter fraction in sediments had a Redfield-like C:N ratio ~ 6, while the less reactive material was depleted in nitrogen (C:N ~ 30-40). However, one particular study on tubes of an infaunal sea anemone, *Ceriantheopsis americanus*, showed that the rates of whole tube decay are 10-100 times slower

than usually found for fresh planktonic debris despite a C:N molar ratio of ~ 5.1 (Kristensen et al., 1991). In central Long Island Sound, these tubes were found to account for a minimum of ~ 0.6–1.8 % and 2.8–8.4 % of the steady state C and N detrital pools in the upper 10-30 cm of sediment (Kristensen et al., 1991). *C. americanus* tube production alone apparently accounted for ~ 9 % of the average particulate carbon and ~ 12 % of the nitrogen fluxes annually to the benthic environment. Tube construction by infaunal benthos may thus represent an important pathway for refractory compound formation and possibly organic matter preservation, and needs to be taken into account in mechanistic models of diagenesis and when attempting to balance sediment budgets.

Burrow walls and tubes of infaunal macro-invertebrates represent one important class of small-scale biogenic structures that are found ubiquitously in sediments (Aller, 1982, Fenchel, 1996). A typical burrow or tube structure is composed of a cylindrical, irrigated shaft that the animal inhabits. The burrow is surrounded by sediment with which the animal interacts. Infauna can construct different types of burrows depending on their mobility. Mobile fauna construct transient burrows of very short residence time, while more sedentary fauna may maintain relatively stable structures for long periods of time. At any given moment, therefore, sediments contain a wide variety of tubes and burrows at various stages of construction, maintenance and disrepair. Many of the burrows formed by infaunal animals are lined with thin layers of organic material, the properties of which may differ from species to species.

Our species of interest, *Chaetopterus variopedatus* is a widely distributed tube forming, suspension feeding annelid of the family Chaetopteridae. *C. variopedatus* studies have been reported as far back as the early 1900s along the coast of North Carolina (Enders, 1909). The worms form tubes from mucus that is secreted from a mucus sac and shaped by the lower lip of the buccal funnel of the worm (Enders, 1909). The tube becomes strengthened from time to time by additional layers of mucus applied to the inside that harden to form a parchment-like material that gives older tubes a laminated structure (Enders, 1909). An illustration of the worm and tube of *Chaetopterus variopedatus* is given in Figure 2 (a). An actual photograph of the tube and worm is shown in Figure 2 (b). A single tube is usually around two feet in length, and ~ 4 cm in diameter at its widest point. The tubes are present in sediments as either U-shaped or oval shaped structures, with two tapering ends sticking out into the water column. The distance between openings can be as great as 50 cm on the surface, and the tubes can penetrate as deep as 25 cm inside the sediment. The linings are diffusively permeable to oxygen (Aller, 1983) and during the course of grab sampling these tubes, it has been noted that the sediment around the tubes is clearly oxygenated (lighter brown in color) if the tube is inhabited or has been recently inhabited. The tube itself is also lighter brown in color indicating the presence of iron oxides. This diffusive permeability to oxygen means that the tube linings can form an oxic-anoxic boundary in sediments and this has the potential to impact the cycling of redox-sensitive metals such as iron and manganese because of the proximity to the irrigated burrow core which acts as a potential source of oxidants.

In coastal embayments like the Chesapeake Bay, *C. variopedatus* has been shown to be an important component of the soft sediment benthic community of lower Chesapeake Bay, and a study conducted in 2000-2001 showed that 35-100 % of the estimated annual net water column production could be linked to the *C. variopedatus* worm population (Thompson & Schaffner,

2001). Of this, 25-60 % was linked to tube production. Tube production can thus play a significant role in the benthic-pelagic coupling of carbon and nitrogen in estuarine systems.

This thesis will attempt to assess the role of *Chaetopterus variopedatus* tube linings in the cycling of organic matter and metals in Long Island Sound, New York. Once abandoned, most tubes are buried in anoxic sediment, and there is no oxygen associated with them. Since these tubes do not build up on the seafloor or in sediments, decomposition would presumably have to take place under anoxic conditions.

II. OBJECTIVES

The primary objective of this study is to quantify the significance of *Chaetopterus variopedatus* tube linings in the overall sedimentary cycling of organic matter in shallow marine deposits. Specific goals include:

- Characterizing the structural properties and chemical environments of tube material and surrounding sediment;
- Assessing the significance of tube linings as a sink for organic matter, and quantify remineralization processes involving tube linings in sediments;
- Assessing the significance of tube linings in the cycling of redox-sensitive metals, specifically manganese and iron;
- Assessing the significance of tube linings in benthic-pelagic coupling.

III. HYPOTHESES

Refractory structural products including tube linings act as a sink for organic matter in marine sediments. These tubes do not build up on the seafloor or in surficial sediments so they presumably decay. However, the pathways for decomposition are uncertain, and initial studies in our laboratory have shown that *Chaetopterus* tube linings, for example, do not readily decay under oxic conditions. Figure 3 illustrates the TCO_2 production rates at specific intervals during oxic incubations of *C. variopedatus* tube linings. Almost no change was observed in the treatment with tubes versus the control (seawater only) over a 250 day period. There was also no obvious visual change in the character of the incubating tube sections. A parallel set of incubations was carried out in anoxic seawater. TCO_2 production from these incubations is shown in Figure 4. It can be seen clearly that there was no major divergence between the control and the treatment with tubes until past day 200. We examined the surfaces of tubes from both these experiments using Scanning Electron Microscopy (SEM) to detect microscopic structural changes, and the most noticeable feature was that tubes in the oxic treatment had micron-sized nodular precipitates on their surfaces. These precipitates were shown by Energy Dispersive X-ray Analysis (EDAX) to be composed primarily of manganese, iron and oxygen (Figures 6 & 8). Qualitatively, the presence of these oxides would be consistent with the brown coloration seen on the surfaces of fresh tubes. In tubes that had been incubated in anoxic seawater these manganese precipitates were clearly absent after day 200.

Based on these preliminary results, we decided to pursue the mechanisms of degradation by following the degradation of tube linings in anoxic sediment under a variety of treatments that would test different hypotheses for degradation.

Hypothesis I: (a) Macrofaunal tube linings have a unique structure and composition that make them more stable under oxic than anoxic conditions, (b) Tube linings of *Chaetopterus variopedatus* have micron-sized metal nodular structures which play a role in preventing degradation.

To address this hypothesis, the decomposition of *Chaetopterus variopedatus* tubes was followed through a set of anoxic sediment incubations. To address the importance of the micron-sized metal precipitates, tube linings were pre-treated with acid to leach the surficial precipitates and the decomposition of these pre-treated tube linings was compared to intact tube linings. Chemical and structural properties of tube linings over the course of degradation were examined in detail through SEM coupled with EDAX, together with detailed analyses of porewater solutes and solid sediment phases.

Surface area is known to play a critical role in determining reactivity of sedimentary organic matter (Hargrave, 1972). In marine sediments, it is possible that the activities of benthos, such as crabs, result in the shredding of tubes and reduction in the size of decomposing material.

Hypothesis II: Tube linings degrade faster when they are broken up into smaller fragments. This might be carried out by grazers such as crabs.

To test this hypothesis, incubation experiments were set up in which the tubes were cut into smaller pieces to simulate shredding by crabs. The decomposition of the pieces was compared to acid-pre-treated tubes and intact tubes.

Ceriantheopsis americanus tubes have been found to account for 9% C flux and 12% N flux in Long Island Sound (Kristensen et al, 1991). Tube production can thus play a significant role in the cycling of nutrient elements. Preliminary elemental characterization of *Chaetopterus* tubes revealed linings with a mole C:N ~ 7.43, C:P ~ 11.3, and enriched in manganese (~ 40X higher than typical estuarine sediments) and iron (~ 2.5X higher than typical sediments).

Hypothesis III: Tube linings are a significant reservoir of nutrient elements and metals and a significant component of elemental and metal cycling in estuarine sediments.

In Chesapeake Bay, *C. variopedatus* has been shown to require 35-100% of net water column primary production to support its existence. ~ 25-60 % of that requirement is attributed to tube formation (Thompson & Schaffner, 2001). The significance of the tubes for areas in Long Island Sound where the worms are found will be evaluated using production-biomass relationships.

IV. EXPERIMENTAL DESIGN & METHODS

Field Methods

Chaetopterus variopedatus tubes were collected by grab sampling in Long Island Sound at the Station P site in September 2008 & September 2010. Tubes were picked out by hand from the sediment grabs and intact, recently inhabited tubes were preferentially selected. The criteria for recent habitation were that either an entire or part of a worm was present in the tube, or the sediment around a tube was visibly oxidized from active irrigation. Mud for the sediment incubations was also collected from Long Island Sound. Specifically, the top 5 cm of sediment were collected, passed through a 1 mm sieve and homogenized before use. Tubes from September 2008 were used for preliminary oxic and anoxic incubation studies, structural studies, amino acid measurements and leach experiments to test the removal of surficial metals. Tubes from September 2010 were used in a set of anoxic incubations described below.

Laboratory Incubations

All incubations were set up using techniques based on a previous study on tubes of *Ceriantheopsis americanus* (Kristensen et al., 1991). Portions of tubes were enclosed in Nytex (nylon mesh) "tea bags" and exposed to specific incubation conditions. For the preliminary oxic water incubations (OXTUB) the tea bags were attached to silicone stoppers and suspended in tall 120 ml glass jars filled with aerated seawater. Magnetic stirrers were included in each jar to agitate the water and prevent the build-up of gradients. All the jars were then submerged in larger polycarbonate containers filled with seawater which was constantly aerated. For the anoxic water incubations (ANTUB) the seawater was purged of O_2 using a N_2/CO_2 mixture. 120 ml jars were then filled with this anoxic seawater, and the jars were sealed with silicone stoppers to which the tea bags were attached.

For anoxic sediment incubations, four experimental treatments were utilized to study the mechanism of degradation of the tube linings (Figure 5 and details below). Controls were set up without tubes. The four treatments were termed SdTUB, PcTUB, LchTUB and Control, reflecting treatments as outlined below.

Worm tubes were rinsed gently in seawater to wash off outer mud coating and cut into ~ 5 cm lengths. These tube pieces were then enclosed in ~ 5.5 cm x 6.0 cm "tea bags" that were prepared from 75 μm Nitex mesh. For the SdTUB treatment, ~ 5 cm length intact tube pieces were used. For the PcTUB treatment, ~ 5 cm lengths were cut into smaller ~ 1 cm pieces and then incubated. For the LchTUB treatment, ~ 5 cm lengths were pre-treated with 1 N HCl for 16 hours to remove surficial metal precipitates and then incubated. On average, each ~ 5 cm length of tube corresponded to a dry weight of ~ 0.09 g tube. From our measurements of average tube C (22 % dry wt), N (7.1 % dry wt) and P (5.0 % dry wt), this corresponds to an extra addition in each jar of about 0.02 gC, 0.0064 gN and 0.0045 gP.

The tea bags were then buried in 60 ml glass jars filled with homogenized sediment. The glass jars were then buried in sealed buckets of mud to maintain anoxic conditions. Jars were sampled every 10-15 days by extracting them from the mud and centrifuging at 2000 rpm for 30 minutes. Porewater was collected after filtering through a 0.2 μm sterile PES filter. At each time point, the pH of the porewater was measured. From day 65 onwards, the sediment pH was also measured. Approximately 0.5-1 ml porewater was analyzed immediately for CO_2 and the remainder sub-divided into two fractions. One fraction was acidified to 10% HCl for analysis of HPO_4^{2-}, Mn^{2+}, Fe^{2+} and Si. The other fraction was frozen and analyzed for NH_4^+ as soon as possible.

The 5 cm lengths collected at each time point were cut into smaller 1 cm lengths and separated for different analyses. 1 cm pieces from each treatment were preserved in 2.5% glutaraldehyde for subsequent SEM analyses. The rest were frozen until use for solid phase CNSP or amino acid analysis.

Chemical Analyses

Porewater from each incubated jar was analyzed for CO_2, pH, NH_4^+, HPO_4^{2-}, silicate, Mn^{2+} and Fe^{2+}. All samples were analyzed in triplicate for each solute. CO_2 was measured using the FIA gas-exchange conductivity method (Hall & Aller, 1991). pH was measured using an Orion pH electrode, which was calibrated and equilibrated for an hour in seawater before each use. Precision for both these measurements was usually better than 2%. NH_4^+, HPO_4^{2-}, silicate, Mn^{2+} and Fe^{2+} were all measured colorimetrically. NH_4^+ and HPO_4^{2-} were measured using the methods cited in Presley, 1971. Silicate was measured by the method given by Strickland and Parsons (1968) and modified by Fanning and Pilson (1973). Mn^{2+} was analyzed by the formaldoxime method proposed by Goto et al. (1962). Fe^{2+} was analyzed by the method given in Stookey (1970). These methods have been modified by Heilbrun et al. (unpublished) for small-volume measurements using a 96-well clear plastic plate and a BMG LabTech plate reader in absorbance mode. Precision for these modified colorimetric methods was usually better than 5%.

SEM Analyses

The tubes were imaged with a Zeiss/LEO 1550 SFEG-SEM at 15 to 20 KeV using a Robinson backscatter detector. Each dried sample was taped to an aluminum substrate using a double-sided carbon tape and coated with several nanometers of gold, to gain electrical conductivity and contrast. Energy Dispersive X-ray spectra (EDS) were collected with an Energy Dispersive X-ray Analysis (EDAX) thin-film window Sapphire detector to identify elemental composition over areas of interest. During this analysis, the specimen is bombarded with an electron beam, and this bombardment knocks out some of the specimen atom's electrons. This vacated position is then eventually filled by a higher-energy electron from an outer shell, which gives up some of its energy in the process by emitting an X-ray. The amount of energy released depends on which shells the energy transfer is occurring between, and each element releases X-rays with unique amounts of energy, so measuring this energy establishes the identity of the element.

Solid phase phosphorus and metal analyses

One centimeter pieces of frozen tube were thawed, gently rinsed with distilled water and dried overnight at 80-90ºC. Sediments were dried overnight as well, though not rinsed with distilled water. Dried tubes & sediments were ground using a mortar and pestle and 3-10 mg were sub-sampled into acid-washed 10 ml glass beakers. One set of dried & ground samples was subjected to a 16 hour 1 N HCl leach, to evaluate the inorganic phosphorus content and the more easily accessible fraction of metals. Another set of samples was ashed at 450ºC for 6 hours followed by a 16 hour 1 N HCl leach, to evaluate the total phosphorus content and the less easily accessible fraction of metals (Aspila et al., 1976). Total dissolved P, Mn^{2+}, Fe^{2+} in the leachates were analyzed colorimetrically as described previously. Al^{3+} was measured using a Perkin-Elmer model graphite furnace atomic absorption spectrometer (GFAAS). Mn^{2+} was analyzed using GFAAS when concentrations were below the detection of the colorimetric method.

Bacterial counts

Total sediment bacteria were counted using a protocol adapted from Hymel & Plante (1998). Briefly, ~1g sediment was sampled from the immediate vicinity of the tube at each time point and stored refrigerated in formaldehyde prepared in 3.5 % NaCl solution to a final concentration of 3% formaldehyde. A 1/10 dilution of this sample was then filtered through a 0.22 µm black polycarbonate filter membrane, and the filter stained with 300 µl 5X SYBR-Gold for 15 minutes. Sediment bacteria were then counted using a Nikon epifluorescence microscope. No bacteria were ever observed on the surface of incubated tube linings, so these were not counted.

Amino Acid Analyses

Amino acids were analyzed using an HPLC protocol adapted from Fleury & Ashley (1983).

V. RESULTS

a. Characterization of *Chaetopterus variopedatus* tube walls

Preliminary SEM studies revealed that there is a definite structure to the *Chaetopterus* tube linings with a distinct cross-woven mesh pattern, which is clearly visible in cross-section as well (Figure 6). The mesh is made out of fibers that are individually 100-200 nm in diameter. The outer tube surface is often occluded by sediment, appears to be rougher and probably reflects the sediment in which the worm tube was first formed. Diatom shell fragments, and sometimes whole diatoms, 5-10 μm across in size are clearly visible. Some examples of these are shown in Figure 7.

Nodular structures 1-2 microns in size were found on the outer surface of the tube linings. Higher magnification also revealed that the "mesh", secreted by the worm on creating the tube, wraps around these nodular structures, suggesting a sedimentary source for the nodular structures. EDAX spectra of these nodules suggest that they are rich in manganese, iron and oxygen (Figure 8).

Chemical characterization of tube linings

C. variopedatus tubes were found to be rich in carbon (C:N ~ 7.43), phosphorus (C:P ~ 11.3), manganese (~ 40X higher than typical estuarine sediments) and iron (~ 2.5X higher than typical sediments). Typical C, N, P concentrations of *C. variopedatus* and other tube linings are shown in Table 2.

Amino acid content of tube linings

Amino acids accounted for ~ 25% of the solid phase carbon and ~ 24% of the solid phase nitrogen in fresh tube linings. The most abundant organic compound measured here was the amino sugar glucosamine, which accounted for ~ 11% solid phase carbon and ~ 7% solid phase nitrogen. Other amino acids that were present in significant amounts were β-alanine, aspartic acid, glutamic acid and glycine. Data for amino acid composition of fresh tube linings and tube linings that were incubated in anoxic sediment for 112 days are given in Table 3. The most significant changes in composition were in the mol % of glucosamine (from 33.1 % in fresh tubes to 22.5 % in incubated tubes) and β-alanine (from 14.6 % in fresh tubes to 8.74 % in incubated tubes).

b. Structural changes during decomposition

Figure 9 shows how the tubes visibly change in color over the course of the anoxic incubations. The primary change is from an initial yellow-brown surface to a blacker surface. SEM and EDAX examinations of the surfaces indicate that the yellow-brown color is most likely due to iron oxides, while the grey-black is almost certainly due to iron sulfides. Qualitatively, this is consistent with the initial oxygenated nature of fresh tubes, discussed earlier in conjunction with their diffusive permeability. Based on these pictures, it is not possible to tell if tubes in one treatment (Sd vs Pc vs Lch) are decomposing faster, but there does appear to be a more definite color change in all treatments around day 65 from yellow-brown to predominantly grey-black.

Figure 10 illustrates the most obvious microscopic change visible on the tube wall surfaces during the course of decomposition – the micro-nodular manganese-rich metal precipitates that are so abundant on un-incubated tubes virtually disappear. The illustration on the left is an un-incubated fresh tube, and the illustration on the right is from day 85 of the PcTUB treatment, but this is a general observation noted for all Sd, Pc and Lch tube linings incubated for at least ten days. EDAX observations of the faint sub-surface whitish micron-sized precipitates on the right show they have relatively very high concentrations of Fe and S, which is the second most obvious visible change. This transition of precipitates is better illustrated in Figure 11, where again the figure on the left is the un-incubated fresh tube and the figure on the right is from day 65 of the LchTUB treatment. Again, this is a general observation noted for all Sd, Pc and Lch tube linings. This is most aesthetically illustrated in Figure 12, which shows several well-formed framboids and cubes of iron sulfide observed on the surfaces of incubated tubes.

Figures 13 & 14 illustrate the most important microscopic change that occurs in the cross-woven organic mesh matrix that is so characteristic of these tube linings. As the tubes decompose, the surface becomes amorphous, as if losing structural integrity compared to the clearly discernible matrix visible in un-incubated fresh tubes shown in Figure 6b. Figure 13 shows that the integrity of the cross-woven mesh matrix is lost as decomposition proceeds. The matrix pattern is still somewhat visible in the lower magnification pictures to the left (10 µm scale bar), but as you zoom in (left to right) the amorphous character of the surface layers becomes apparent. The cross-section in Figure 6a shows the layered nature of these tube linings, and Figure 13 also illustrates an interesting point about the decomposition of different layers. The top row in Figure 13 is the outer-most surface of the tube lining in this SdTUB treatment at day 28, the middle row is one layer down and the bottom row is yet another layer down. If we compare the right-most column of pictures (1 µm scale bar) it is evident that the outer-most surface is the most amorphous and that the integrity of the mesh matrix in the innermost layer is still intact. Thus the inner layers are slower to degrade in SdTUB treatments, as they are only exposed to degradation once the outer layers start decomposing.

In Figure 14, similar pictures are shown for different layers in the PcTUB treatment sampled at the same time (day 28). As in Figure 13, top to bottom is outer-most layer to innermost layer. It is evident that in the PcTUB treatments the tube linings are amorphous even in the innermost layers, which supports the hypothesis that the tube linings degrade faster when

they are shredded, as more surface area is exposed for decomposition. As more surface area is exposed, the manganese released from reduction of the micro-nodular precipitates also has a chance to diffuse away from a greater surface area, while in the SdTUB treatment the manganese is more likely to stay within the tube for a longer period of time. This is corroborated by measurements of total solid phase manganese in tubes over the incubation time-course (discussed in a later section).

The increase in amorphousness over time is also illustrated in Figure 15, which consists of pictures of outer to inner layers of tube linings from day 65 of the SdTUB treatment. Comparing these to Figure 13, it is clear that even the inner layers are amorphous by this time, showing that the organic matrix has lost its structural integrity even in inner layers by day 65.

c. Stoichiometric relationships between C, N and P

Changes in porewater CO_2, NH_4^+ and HPO_4^{2-} over the incubation time course are shown in Figures 16 through 18 respectively. For all three, there seems to be a steeper rise in porewater solutes through the first ~ 64 days after which the rise slows down for TCO_2 and almost flattens out for NH_4^+ and HPO_4^{2-}. This is typical of sediment pools in which one of three possibilities might be occurring: (1) there are multiple pools and there is a loss of the most reactive substrate by day 64, (2) there is one pool which is running out over time, but this is not the most likely explanation here as the tubes are still visibly present even after 125 days, (3) there is inhibition of organic matter remineralization due to the build up of metabolic by-products. Thus the conceptual interpretations differ for different regions of each of the curves, and perhaps the most logical solution is to consider the initial rate behavior as most accurately reflecting how the tube linings affect organic matter remineralization in sediments. From these observations, the time scale for release of organic matter from the tube linings appears to be on the order of ~ 65 days. The production numbers for C, N and P are significantly different from the control experiment in all cases. The linear regression slopes of these production values for day 0-64 are summarized in Table 4. Production values for day 64-125 are listed in Table 5.

CO_2 production goes in the order SdTUB ≈ LchTUB > PcTUB > control. NH_4^+ production goes in the order LchTUB > PcTUB > control > SdTUB. However, the SdTUB NH_4^+ seems to flatten out earlier than 64 days, so a linear regression was performed for SdTUB from 0-51 days instead, and with the revised estimate, the NH_4^+ production goes in the order LchTUB > SdTUB ≈ PcTUB > control. HPO_4^{2-} production goes in the order LchTUB > SdTUB > PcTUB >> control. The HPO_4^{2-} production in particular is not surprising because the phosphorus content of the tubes is so high in the first place, being on average around 5% of the dry weight of the tubes. It should be mentioned here that in studies detailing the various pools of phosphorus in the tubes (using the SEDEX method, Ruttenberg 1992), the majority of the phosphorus in the tubes was found to be contained in the organic phase, and therefore is not removed by the acid pre-leach in the LchTUB treatment. Overall, these production estimates would suggest that on a timescale of 64 days, the acid-pre-treated tubes decay the fastest, followed by the whole tubes and then the pieced tubes. It is worth noting that from day 64 to 125, it is the PcTUB treatment that shows the most significant overall linear production of CO_2 and NH_4^+ while the others almost flatten out (Table 5).

Plots of C:N (Figure 19) show that the control sediment exhibits Redfield-like ratios for CO_2:NH_4^+ release (7.00). This data is summarized in Table 6. The SdTUB treatment has a higher ratio (9.40 for days 0-64 or 7.61 for days 0-51), whereas the PcTUB and LchTUB treatment ratios are 6.01 and 6.60 respectively. All C:P plots (Figure 20) reveal ratios that are 3.5-5X lower than Redfield ratios, showing a huge amount of phosphorus release and enrichment in these sediments. The order of C:P ratios is SdTUB (29.72) > LchTUB (25.63) > control (24.54) > PcTUB (21.01). Somewhat surprisingly, the control experiment without tubes also exhibits huge phosphorus enrichment.

The difference between SdTUB and PcTUB for both C:N and C:P plots is on the order of 30%, which shows that much more ammonium and phosphate is released from shredded tubes compared to the whole tubes during the process of decomposition.

Solid phase measurements of phosphorus in tubes and sediment are shown in Figures 21. The most important thing to be noted is the >30X enrichment of P in tubes compared to surrounding sediments. Except for small fluctuations, neither changes much over time, though there is a ~25% decrease in sediments compared to the initial t0 value, and a ~22% increase in tubes compared to the initial t0 value. The directions of these changes are somewhat surprising given the initial enrichment in tubes compared to sediments, and the steep concentration gradient that would be expected as a result. However, most of the phosphorus in the tubes is actually present in the organic part of the mesh matrix (>98% organic P and <2% inorganic P) and thus remains firmly bound in the tube until the tube decomposes completely, at a time scale greater than that followed in this series of experiments. In the sediments, the distribution of phosphorus is on the order of 50% in each of the inorganic and organic pools, at concentration ranges of 20-25 µmoles/g in each pool (data listed in Appendix).

The cycling of phosphorus is also potentially related to iron cycling in sediments, though no significant relationships were found between porewater HPO_4^{2-} and Fe^{2+}. Analysis of solid Fe and P in sediments showed some significant relationships, shown in Figure 25 and summarized in Table 7. Inorganic phosphorus is most tightly correlated with more easily accessible Fe (defined as the solid Fe extracted by a 16 hr 1 N HCl on dry tubes/sediment).

d. Manganese and iron cycling in sediments in the presence of tube linings.

Porewater Mn^{2+} and Fe^{2+} generally increase over the incubation time course (Figure 23). Mn^{2+} levels are elevated in treatments with tubes compared to control sediment. The Fe^{2+} data are extremely noisy and no clear inferences can be drawn from them. Reducing conditions result in Mn^{2+} release from the tubes into pore water. These observations are consistent with the loss of Mn-rich micro-nodules during anoxic incubations. An inorganic source for Mn is also consistent, but not uniquely so, with lower Mn release from material pretreated with HCl, where a significant amount of Mn (>60%) was pre-leached off these tubes before incubation. Changes in solid phase Mn in tubes and sediment are shown in Figure 24. In all tube incubations, the Mn content in the residual tubes decreases over time, with the total overall Mn content generally remaining highest in the SdTUB treatment. Even at the lowest total tube Mn values (4000-18000

µg/g), tubes are still 8-20X more enriched compared to total solid Mn in surrounding sediment, which stays approximately constant around 500 µg/g. Thus there is potentially a substantial concentration gradient to drive Mn away from the tubes as it is released upon tube decomposition.

Despite the approximate average value, there are small differences in total sedimentary Mn in the different treatments (non-tube total Mn), and this is emphasized in Figure 25 in which total Mn in sediments is plotted against porewater Mn^{2+}. There is a direct relationship between the two in the case of SdTUB and PcTUB treatments compared to the control and LchTUB treatments. This reinforces the point that Mn in porewater is derived from the highly manganese-rich tubes, and that the Mn released from the tubes also increases the total Mn in surrounding sediment. The control and LchTUB treatments show different results, and can be interpreted in different ways. In the control treatment, the sediment must be the source of dissolved Mn^{2+} in porewater, and this is verified by the inverse relationship between solid Mn and porewater Mn. However, in the LchTUB treatment, the tubes must be the source of porewater Mn^{2+} as the sediment Mn does not increase over the course of the incubation. The quantity of Mn involved in this case is not sufficient to detectably increase total Mn in surrounding sediment. This second point is also clear in the lower panel of Figure 24, which shows that the overall average value for Mn in sediments is lowest for the LchTUB treatment. Table 8 summarizes the geometric mean slopes and p values for the trendlines shown in Figure 25. There is no clear significance for the slope values, though the general behavior is clear from the magnitudes and signs of the slopes.

Changes in solid phase Fe are shown in Figure 26. >35% of the Fe is removed in the acid pre-leach in LchTUB treatments. As with Mn, there is a decrease in Fe, however this occurs only at the beginning, and after day 28, the Fe content in the incubated tubes stays approximately constant. This corroborates the observations of iron pyrite formation on the tube surfaces, showing that the iron doesn't exit the tube so much as change into a different solid phase. The average value for both tubes and sediment after day 28 is around 15,000 µg/g, so there is no concentration gradient to drive Fe away from the tubes as there is in the case of Mn. Also unlike Mn, there is no clear relationship between the total solid Fe in sediments and porewater Fe^{2+}, shown in Figure 24 with the geometric mean slopes and p values listed in Table 8.

To distinguish between authigenic and lithogenic Mn and Fe, we measured total Al in tubes and sediments. These data are plotted in Figures 28 and 29 for Mn and Fe respectively, and geometric mean slopes of these data are summarized in Tables 9 and 10. The tightest correlation is for sedimentary solid Fe and Al.

The average Mn/Al wt ratio for control sediments is 0.04, which is 8X higher than values reported for shale (0.01, Turekian & Wedepohl, 1961). The average Mn/Al for un-incubated tubes is 7.21, and while the Mn/Al for incubated tubes decreases over time, the average values of 5.62, 4.44 and 3.02 (for Sd, Pc and Lch respectively) are 300-560X higher than values reported for shale. The sediments sampled from tube incubation jars shows some enrichment as well compared to both shale values and the control sediment. The lowest value is for the LchTUB treatment, in which the average value is very similar to control sediment. SdTUB and PcTUB treatments show 15 and 19% more enrichment compared to control sediments, another indication that Mn in these sediments is being sourced from the tubes.

The average Fe/Al ratio for control sediments is 1.27, which is ~2X higher than values reported for shale (0.59, Turekian & Wedepohl, 1961). The average Fe/Al for un-incubated tubes is 11.6, and the average values of 9.10, 8.25 and 9.45 (for Sd, Pc and Lch respectively) are 14-16X higher than values reported for shale. As with Mn, the sediments sampled in the tube incubation jars showed some enrichment compared with control sediments. The least enrichment was in the SdTUB experiment, which was ~1.6% higher. PcTUB sediments were ~5.6% higher and LchTUB ~10.4% higher.

VI. DISCUSSION

a. Structural changes during decomposition

The cross-woven mesh matrix observed in *Chaetopterus variopedatus* tube linings is characteristic of tube linings made by several other species of estuarine tube-secreting worms. Some examples of these are shown in Figure 30, which includes SEM photos taken of linings of Axiothellae, Diopatra, Onuphis and Chaetopterus tubes sampled in the North Inlet backbarrier intertidal region in South Carolina in 1982 (kept frozen at -20ºC since collection). Some, such as Axiothellae, are found in sandy sediments, as opposed to the muddy LIS sediments from which Chaetopterus tubes for this thesis were sampled, however all display a cross-woven mesh-like background structure.

Despite the common mesh-like background matrix, there is a distinct absence of micro-nodular precipitates of any kind visible in the photos of Axiothellae, Onuphis and Diopatra. Chaetopterus tubes collected in South Carolina showed some manganese micro-nodular precipitates on the surface (Figure 30), though not as abundant as the ones observed on LIS Chaetopterus tubes collected in September 2010. This difference in abundance is probably due to the fact that Chaetopterus tubes sampled in South Carolina were from sediment that was sandier than Long Island Sound, and thus lower in Mn available for diagenetic remobilization. Based on these observations and a search of available literature, it would seem that Chaetopterus tubes are unusual with regard to these micro-nodular manganese precipitates. A potential mechanism for the production of these micro-nodular precipitates may be deduced by examining their location. From Figures 6d & 6e it can be seen that the precipitates tend to track the mesh pattern of the background matrix, and it is possible that the precipitates are formed in that pattern by Mn^{2+} diffusing into the "holes" of the matrix and meeting O_2 (from seawater circulated by irrigation) diffusing outward. EDAX spectra of the micro-nodular precipitates confirms high levels of oxygen in the precipitates, in addition to Fe and smaller amounts of Ca, Mg etc. On the surface of tubes that were left in oxygenated seawater for over 6 years at room temperature in our laboratory, we observed that these precipitates grew as large as 25-30 microns. Those particular 6-year old tubes were still intact and structurally robust, demonstrating the stability of these tube linings under oxic conditions, and hinting at the possible stabilizing role of these surface precipitates. This stability under oxic conditions was also demonstrated by our initial experiments with tubes in oxygenated seawater (Figure 3). It is also possible that the polymer structure acts as a template to nucleate micro-nodules.

The precipitation of these micro-nodules at the matrix "holes" could serve to strengthen the matrix through cross-linking, and the removal of these precipitates through reduction over the course of our incubation experiment could be a direct chemical reason for weakening and subsequent degradation of the matrix. SEM pictures of leached tubes show this in Figures 31a & 31b. The surface matrix appears to be more spread apart than SdTUB and PcTUB treatments at similar time points, and the tube walls have lost a substantial amount of their surface structural integrity by day 37. This also suggests that the degradation of tube linings in the environment

may be linked to the onset of anoxia in bottom waters in late summer months in estuaries where these tubes are found.

b. C, N, P remineralization and stoichiometric relationships

It is clear from the incubation experiments that there is elevated production of CO_2, NH_4^+ and HPO_4^{2-} in the presence of tubes compared to control sediments (Table 4). From Table 2, it is also clear that the production over days 0-64 is highest for CO_2, NH_4^+ and HPO_4^{2-} in the LchTUB treatment (assuming that both SdTUB and LchTUB CO_2 production are approximately equal to 0.24 mM/day). It is somewhat surprising that production values for SdTUB are higher than PcTUB, since one of our hypotheses was that shredding the tubes would increase their decomposition rate, and our SEM observations showed more loss of structural integrity on the edges of shredded tubes versus whole tubes. However, PcTUB CO_2 and NH_4^+ production also continues to increase significantly from day 64-125 (Table 3) while LchTUB appears to plateau. SdTUB CO_2 production also continues to significantly increase, though at a lesser rate compared to the first 64 days, but SdTUB NH_4^+ production also flattens out. It is possible to explain these observations if we imagine that in the PcTUB experiment there is more labile organic matter available for a longer period of time (through greater exposed surface area), and the organic matter remineralization is not as sharply 2-step as SdTUB and LchTUB, in which the degradation of the top layer takes on the order of 65 days but the inner layers take longer to be fully exposed and then degraded.

From stoichiometric relationships shown in Table 6, PcTUB and LchTUB treatments release much more NH_4^+ and HPO_4^{2-} versus CO_2, in contrast to SdTUB which releases much more CO_2 versus NH_4^+ and HPO_4^{2-} compared to control sediments. This would indicate that the N and P pools in the PcTUB and LchTUB treatments are more accessible to degradation, and are perhaps being released from edges or inner layers of tube linings that are more exposed to degradation earlier compared to the SdTUB treatment where the majority of remineralized organic matter is from the topmost surface of the tube linings.

One of the more interesting aspects of elemental composition of these tube linings is determining which phosphorus compounds are involved in making the C:P ratio so low. One possible explanation stems from observations of phosphorylation reported recently in both marine and aquatic species (Stewart et al., 2004, Stewart & Wang, 2010). In the marine polychaete *Phragmatopoma californica*, the tube cement that goes into making the polychaete's hardened tubes was found to contain >28 mol% of phosphoserine, with >90% of the serine residues being phosphorylated (Stewart et al., 2004). In several aquatic caddisfly species, the characteristic H-fibroin was found to be densely phosphorylated with >50% of the serine residues being phosphorylated (Stewart & Wang, 2010). In the latter study, the authors proposed that phosphorylation of serines, which are also present in moth and butterfly terrestrial cousins, is an evolutionary method for adapting a dry ancestral silk to the underwater environment of caddisfly larva. Our amino acid measurements did not detect phosphoserine, but as in the case of glucosamine, this is probably because of hydrolysis of the phosphoserine during the preparatory step. There is a slight net increase in Ser (from 3.0 to 3.3 mol%), but since this is a net change, it

is not possible to confirm that phosphoserine is the source of the increase. An alternative method will have to be employed to quantify phosphoserine concentrations in tube linings.

c. Manganese cycling in the presence of tube linings

From solid CNS and metal data, it is clear that the worm tubes act as sinks not only for carbon, nitrogen and phosphorus – with P being much more enriched than phytoplankton – but also for redox metals and manganese in particular. The ~40X Mn enrichment compared to surrounding sediments, and the 300-500X enrichment compared to lithogenic manganese, seems to be unique to *Chaetopterus* tube linings compared to other ubiquitously found worm tubes. There are many other metals to be found in estuarine sediments (Fe and Ca for example) that are also capable of cross-linking and stabilizing the mesh matrix. In fact, Ca has been reported as a cross-linker in bio-adhesives in marine sand castle worms, silk worms and caddisfly larvae (Stewart et al., 2004, Sun et al., 2007, Stewart & Wang, 2010). So why should manganese be the metal of choice?

As far back as 1922, Cyril Berkeley reported that tubes of *Mesochaetopterus Taylori* (sampled in British Columbia) and *Chaetopterus variopedatus* (sampled at Woods Hole) contained very high amounts of manganese (~0.02% by weight for *M. Taylori* and ~0.45% by weight for *C. variopedatus*) (Berkeley, 1922). He sampled tissue from both worms and found the manganese to be about 0.01% by weight in both sets of tissues. He concluded that the manganese in tube walls must be a secretory by-product from the worms, especially so in the case of *M. taylori* where he measured the highest tissue manganese concentrations in the median region of the body which contains the mucus secreting glands. He acknowledged that in the case of *C. variopedatus* the concentrations in the tube walls were significantly higher. *Sabellid* and *spiochaetopterus* tubes examined by him were found to contain no manganese. *C. variopedatus* tube wall manganese concentrations in our study were on the order of 2-3% by weight, and we did not collect tissue samples of live worms so it is not clear whether the Mn is a secretory by-product in our system. However, given the ~40X Mn enrichment compared to surrounding sediments, it can be easily imagined that the worms must live in a very Mn-rich environment within their tubes, and moreover must be able to either flush out or tolerate these elevated levels of manganese, which can be toxic in large doses (Gerber et al., 2002). Antibacterial properties of manganese complexes have been studied (Geraghty et al., 2000, Mandal et al., 2011) and its toxicity has been utilized in the production of anti-bacterial bandages (Farrah & Erdos, 1991). Is it possible that *Chaetopterus variopedatus* worms have harnessed this anti-bacterial property to their advantage? Our evidence from thousands of SEM pictures taken so far of these tube walls supports this theory – not one single bacterium has been observed on the surfaces of these tubes. So while bacteria happily grow and decompose extremely labile organic matter such as fresh plankton, perhaps they are actively deterred from attacking the tube wall surfaces by the presence of such high concentrations of manganese.

There is another process, however, that might explain the presence of these micro-nodular manganese precipitates and still involve bacteria directly. Ever since the discovery of manganese nodules on the deep sea floor, the origins of these nodules have been a great source of debate. Both abiogenic and biogenic pathways have been theorized (Jauhari & Pattan, 2000,

Zhang et al., 2002), and a recent paper by Wang et al. (2009) showed through high-resolution scanning electron microscopy of sectioned nodules that endolithic microorganisms exist and are arranged in a highly organized manner on mineral plane surfaces within the nodules. It would be interesting to section the micronodular precipitates that we see on *C. variopedatus* tube linings and examine them for similar endolithic microorganisms. If these microorganisms were found to exist, that would suggest a biogenic origin to these nodules.

d. Amino acid composition and total sedimentary bacteria

Preliminary amino acid analyses of *C. variopedatus* tube linings showed extremely high levels of the amino sugar glucosamine (~ 33 mol% in fresh tubes, Table 3), which is a common mucopolysaccharide secreted by marine animals (Bunde et al., 1978). In fact, amino acids account for at least ~25% of solid phase C and ~24% of solid phase N in fresh tubes, with glucosamine accounting for ~11% of the total solid phase C and ~7% of the total solid phase N. It must be pointed out that this is probably an underestimate at best, since experiments by Tang et al (unpublished) revealed that a substantial amount of glucosamine decomposes during the amino acid preparatory hydrolysis step in the procedure we used. Other amino acids found in relatively high concentrations were aspartic acid (~ 9.6 mol%), glutamic acid (~ 5.6 mol%), glycine (~ 7.9 mol%) and ß-alanine (~14.6 mol%). The first three qualitatively match the major amino acids reported in organic matter contained in tube walls of marine serpulid worms (Gaill & Hunt, 1988, Tanur et al., 2010) although both those studies also reported significant concentrations of proline, which our method does not detect. The most significant changes in amino acid concentrations over the course of anoxic sediment incubations of *C. variopedatus* tube material were decreases in glucosamine (from ~33 mol% to ~23 mol% over 112 days) and ß-alanine (from ~15 mol% to ~ 8.7 mol%). The former is almost certainly related to decomposition of the organic material in the tube linings. As for the latter, ß-alanine is an indicator of diagenetic changes (Lee & Cronin, 1982) and usually increases as organic matter degradation proceeds (Cowie & Hedges, 1992, 1994) so it seems unusual that it would decrease as degradation of the tube linings proceeds. However the loss of this ß-alanine could be linked to the loss of micro-nodule-related bacteria, if those bacteria were shown to exist. ß-alanine produced by bacteria in sediments is also labile, and if the rest of the worm tube amino acids were not available then it would be preferentially used.

Measurements on the total sediment bacteria in a previous set of anoxic sediment incubations with tubes showed no significant difference in total bacterial counts over an extended time period between sediments sampled immediately adjacent (<0.5 cm distance) to teabags with and without tubes (Figure 32). The initial increase is likely due to the initial handling (mixing and sieving) during homogenization of sediment. Thereafter the numbers stay constant around 5-6 x 10^8 bacteria/g dry sediment. Therefore, it seems that sedimentary bacterial numbers are unaffected by tube decomposition, at least immediately adjacent to the tubes. It is possible that the decomposition is being carried out via extra-cellular enzymes released by bacteria that are further away from the tubes. In any case, it is unlikely that bacteria would be able to directly access the organic matter on the tubes unless it was first broken down into smaller pieces that were less than the typical size limit (600 Da, Weiss et al., 1991) for uptake by heterotrophic microbes. Arnosti et al. (1994) demonstrated rapid enzymatic hydrolysis of high

molecular weight polysaccharides under anaerobic conditions, and even showed that, given the presence of the right consortium of bacteria to produce the extra-cellular enzymes, rates of this enzymatic hydrolysis could be faster than bacterial uptake of remineralized components. It would be interesting to repeat this series of experiments and look at variations in extracellular enzymes in incubated sediments during the first sixty-five days.

e. Benthic-pelagic coupling

C. variopedatus feeds by filtering particles from seawater which it constantly flushes through its tube habitat, thus transforming more or less labile organic material from seawater into relatively refractory structures during tube construction and maintenance, similar to *C. americanus* described in Kristensen et al. (1991). The role of *C. variopedatus* tubes in benthic-pelagic coupling can be assessed roughly by examining production rates and biomass relationships. Our primary assumptions concerning production and biomass relationships come from a previous study on *C. variopedatus* worms and tubes in the Chesapeake Bay (Thompson & Schaffner, 2001). They reported a mean density of ~100 individuals m^{-2} and a tube production rate of 13.6 gC m^{-2} yr^{-1}. They report a C/AFDW ratio of 0.55 while the tubes in our study had a C/AFDW ratio of 0.32. Correcting for this ratio gives us a tube production rate of 7.9 gC m^{-2} yr^{-1} for *C. variopedatus* tubes in Long Island Sound, given the same abundance. Values for average C, N and P content for our tubes were 22%, 3.6% and 5.2%, and these give corresponding tube production rates of 1.27 gN m^{-2} yr^{-1} and 1.82 gP m^{-2} yr^{-1}. If we assume that 64 gC m^{-2} yr^{-1} or 31% of the primary production in Long Island Sound (205 gC m^{-2} yr^{-1}) is available for benthic organisms (Riley, 1956), the production of *C. variopedatus* tubes could consume on the order of ~12% of the average annual benthic carbon supply, ~11% of the nitrogen flux and >100% of the phosphorus flux (assuming Redfield source C:N ~ 6.7 and C:P ~ 106). *Chaetopterus* tubes are not uniformly distributed throughout Long Island Sound and there are no recent benthic surveys that accurately assess their abundance. Thus these percentages are at best local estimates of what might occur, but they still indicate that a single species can modify a substantial proportion of annual benthic fluxes in these localized areas.

VII. CONCLUSIONS

- *C. variopedatus* tube linings are extremely rich in phosphorus compared to organic matter with a Redfield average stoichiometry. The most reactive part of this organic matter is remineralized on a time scale of about 65 days when exposed to sediment under anoxic conditions. Thus the tube linings substantially alter the cycling of C, N and P compared to control sediments during this 65-day period.

- There are significant changes in visible and microscopic structural composition of *C. variopedatus* tube linings during decomposition: (1) transition from Mn-based micronodular precipitates and iron oxides to FeS_x or straight sulfur, (2) discernible loss of structural integrity of the mesh matrix, (3) evidence for spatially progressive degradation rather than pervasive decomposition.

- *C. variopedatus* tube linings are extremely rich in Mn compared to average estuarine sediment as well as lithogenically sourced Mn. This Mn is released from the surface of the linings on a time scale of 2-3 weeks and substantially alters porewater and sedimentary Mn cycling.

- Potential mechanisms for Mn micronodular precipitates stabilizing tube linings are direct crosslinking or bacterial deterrence.

- In localized areas where they are found in abundance, *C. variopedatus* tube production can account for ~12% of the average annual POC flux, ~11% of the PON flux and >100% of the POP flux to the benthos. These tubes are mostly found in muddy sediments, which comprise about 60% of the total seafloor area in Long Island Sound (Poppe et al., 2009), so tube production could potentially account for fluxes in up to 60% of the bottom waters of Long Island Sound.

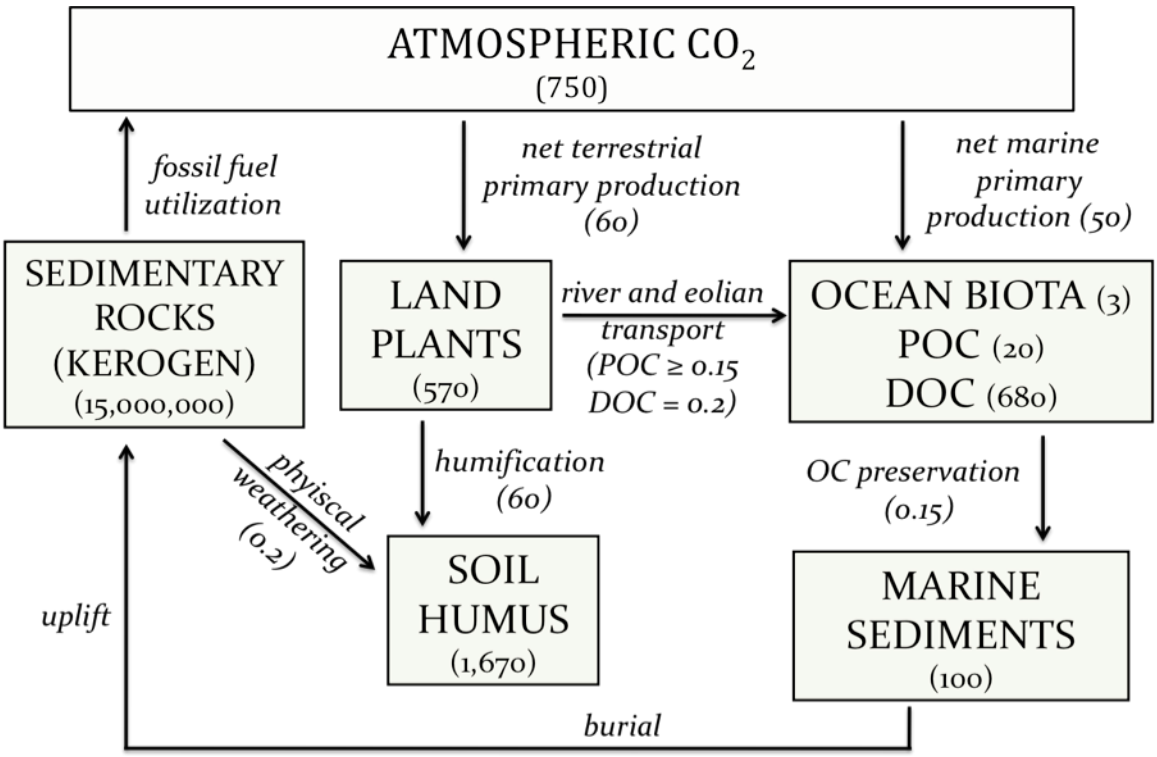

Figure 1: The organic carbon cycle (adapted from Eglinton & Repeta, 2004). Numbers in parentheses are amounts in Gt of Carbon (1 Gt = 10^{15} g C).

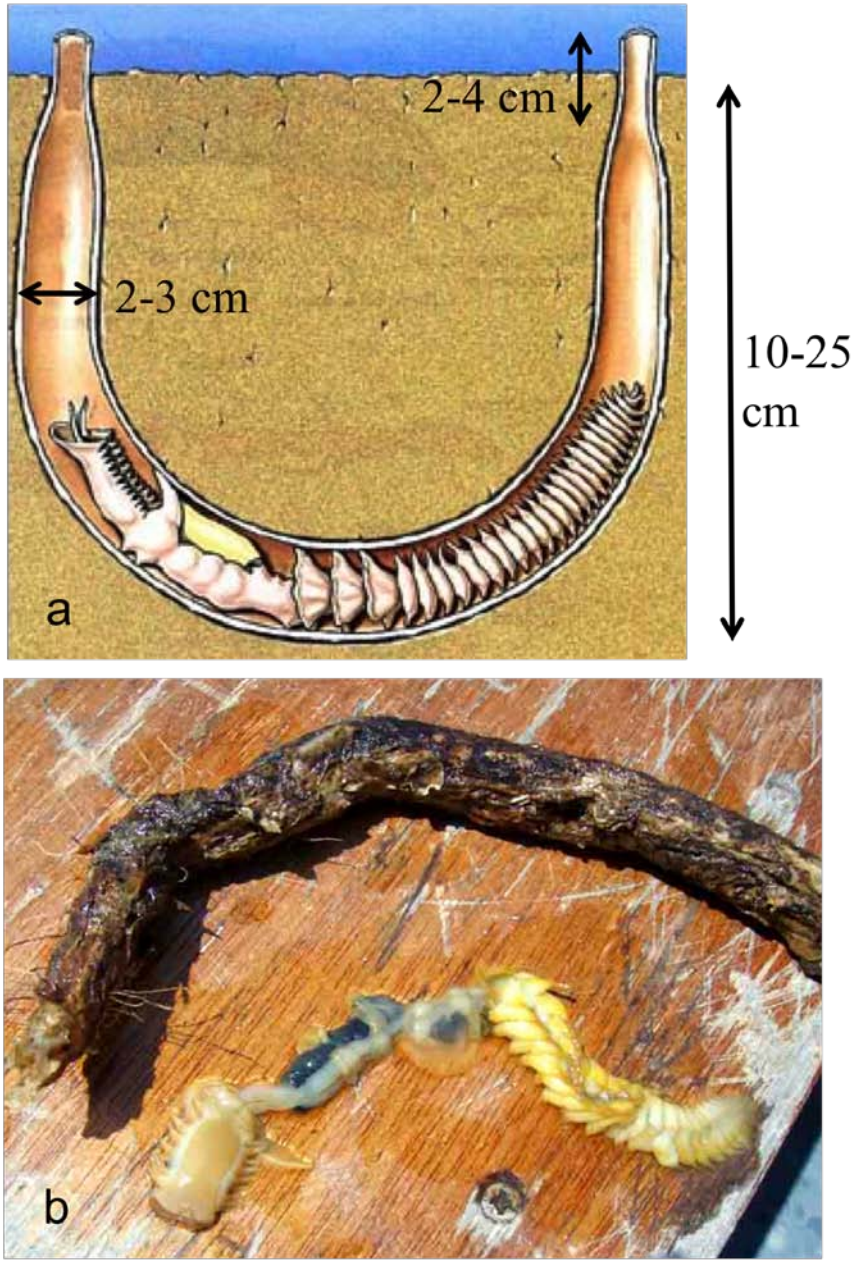

Figure 2: Illustration of *Chaetopterus variopedatus* tubes and worms. (a) Cartoon of worm in tube in sediments. Characteristic scales are shown. (Gillis and Haro, 2010), (b) Picture of tube and worm recently extracted from sediment (Sewell 2002).

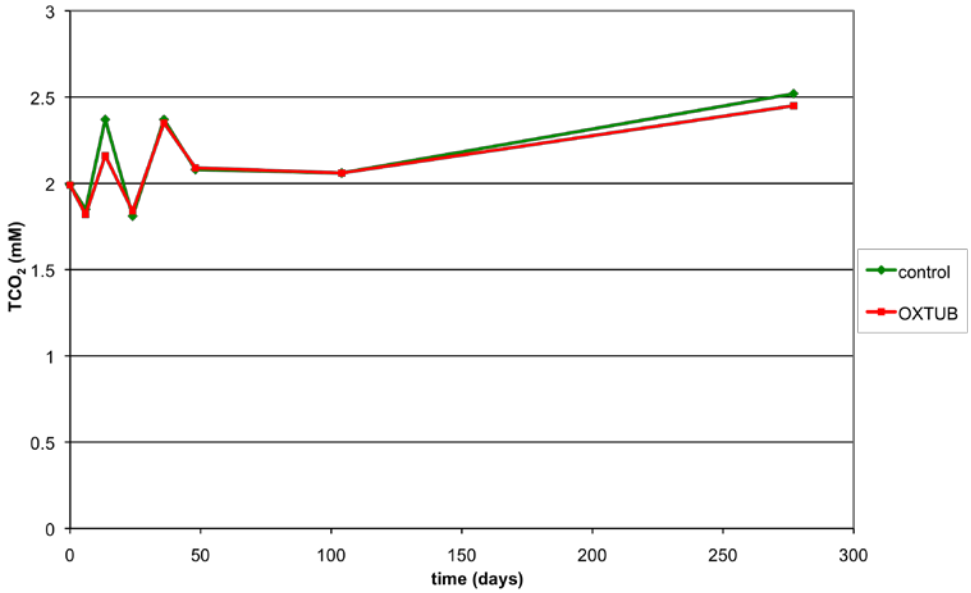

Figure 3: TCO_2 production during oxic incubations of *C. variopedatus* tube linings. OXTUB = tubes in oxygenated seawater, control = seawater without tubes.

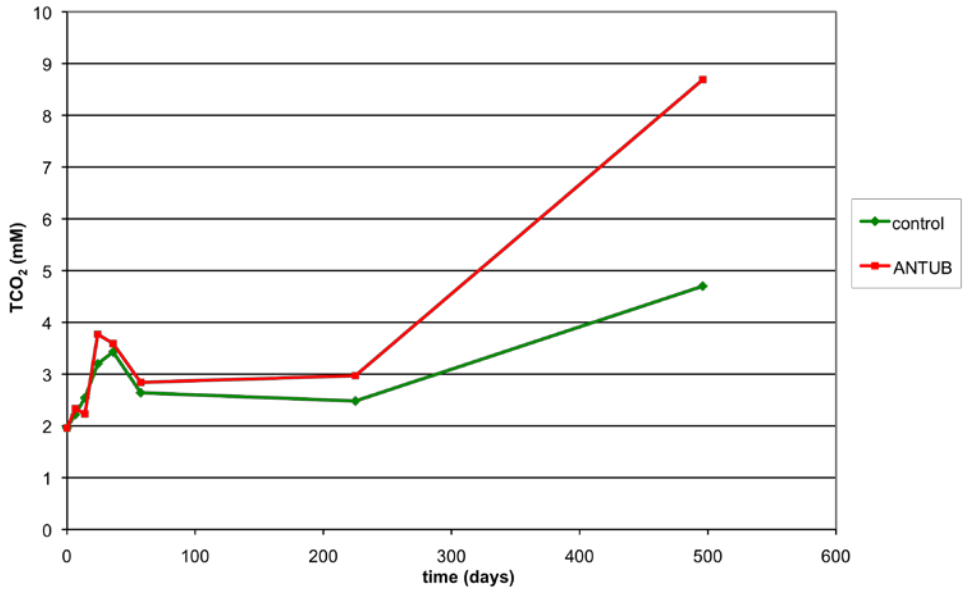

Figure 4: TCO_2 production during anoxic incubations of *C. variopedatus* tube linings. ANTUB = tubes in anoxic seawater, control = anoxic seawater without tubes.

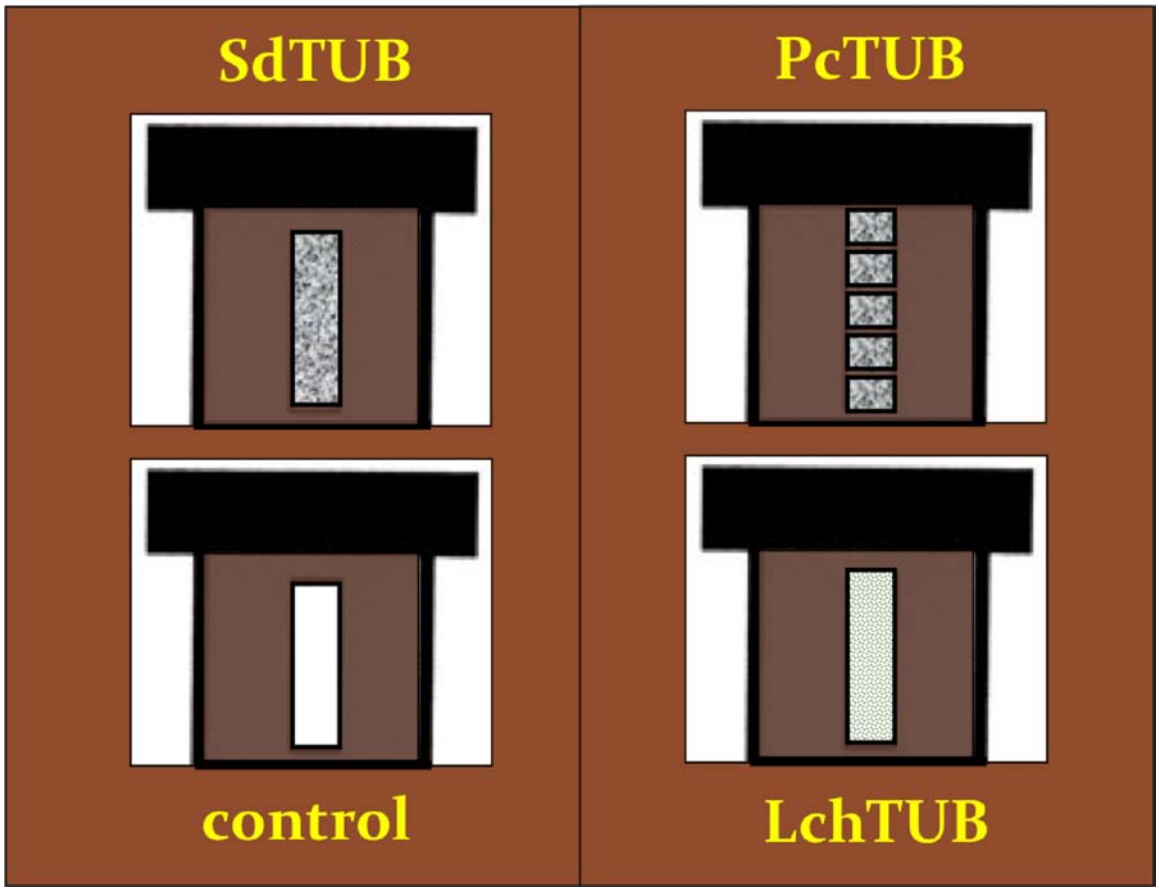

Figure 5: Anoxic sediment incubations of *C. variopedatus* tube linings. In each experiment, tube pieces were enclosed in 75µm Nitex mesh tea bags.
SdTUB – 5 cm lengths of tube linings; PcTUB – 5 cm lengths of tube linings cut into smaller 1 cm pieces; LchTUB – 5 cm lengths of tube linings which were pre-treated with acid to leach off surface precipitates; control – tea bags only.

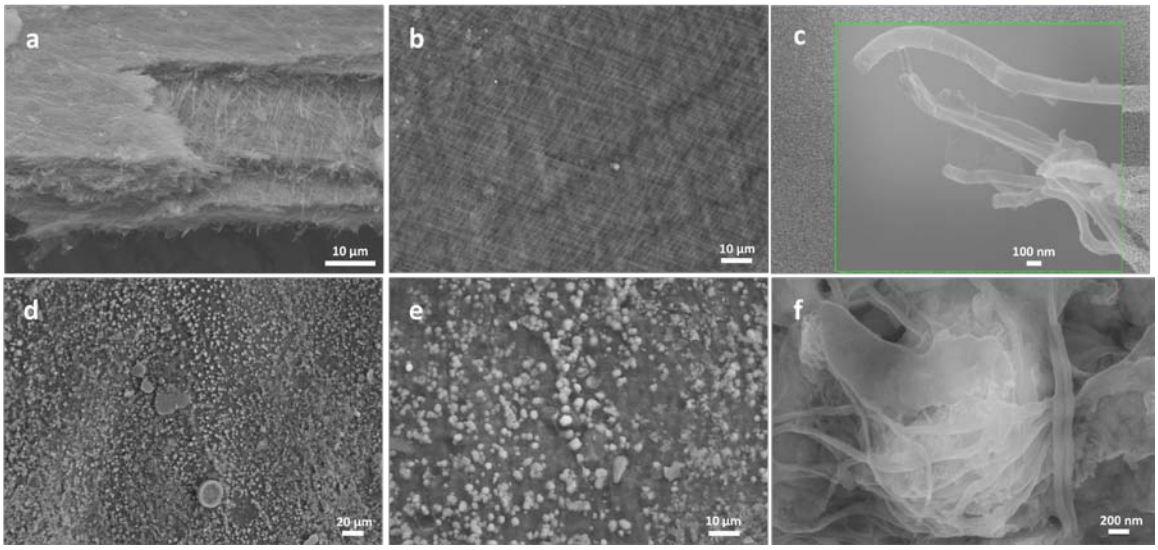

Figure 6: Scanning Electron Microscope pictures (a-f) of *C.* var*iopedatus* tube walls; (a) cross-sectional view showing the presence of multiple thin layers, each a few microns wide, (b) top view of mesh-like pattern, (c) close-up of individual fibers, (d) & (e) manganese micro-nodular precipitates on tube surface, demonstrating how these precipitates track the fibrous background matrix, (f) close-up illustrating that the micro-nodular precipitates are woven into the mesh and not just adsorbed on the surface.

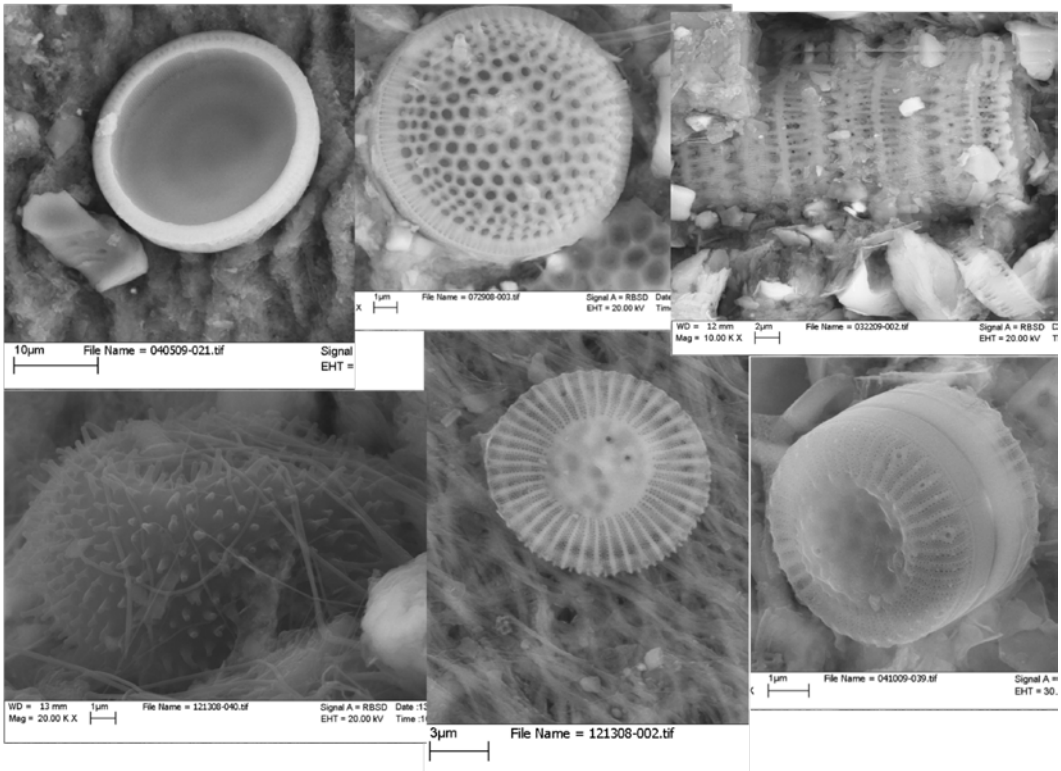

Figure 7: An assortment of diatoms seen on the surface of *C.* var*iopedatus* tube walls.

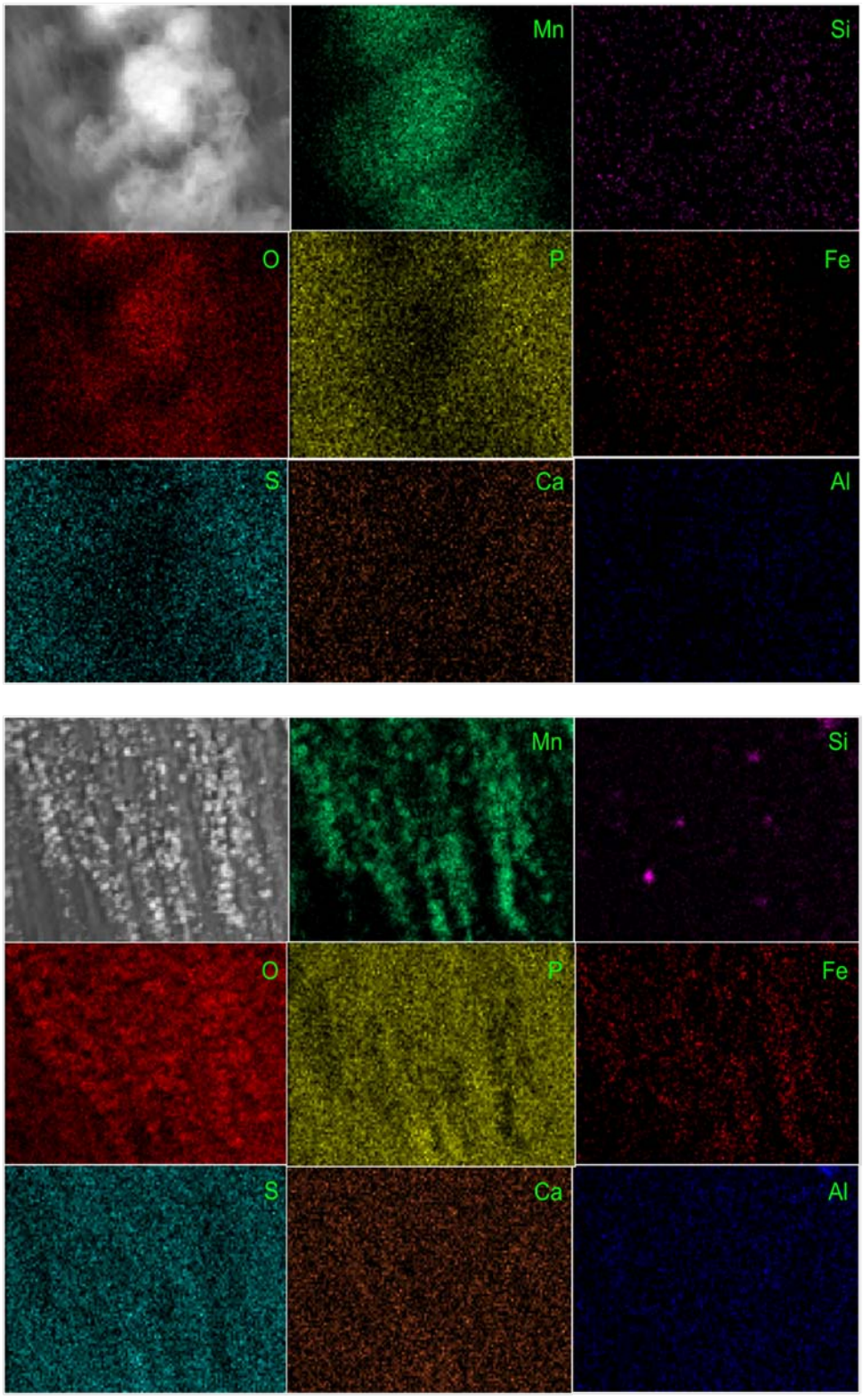

Figure 8: 2-D EDAX spectra of *C.* va*riopedatus* tube walls, illustrating the relative elemental concentrations of the surface precipitates and the surrounding fibrous matrix. (top) single micron-sized precipitate, (bottom) 625 μm^2 area showing several precipitates.

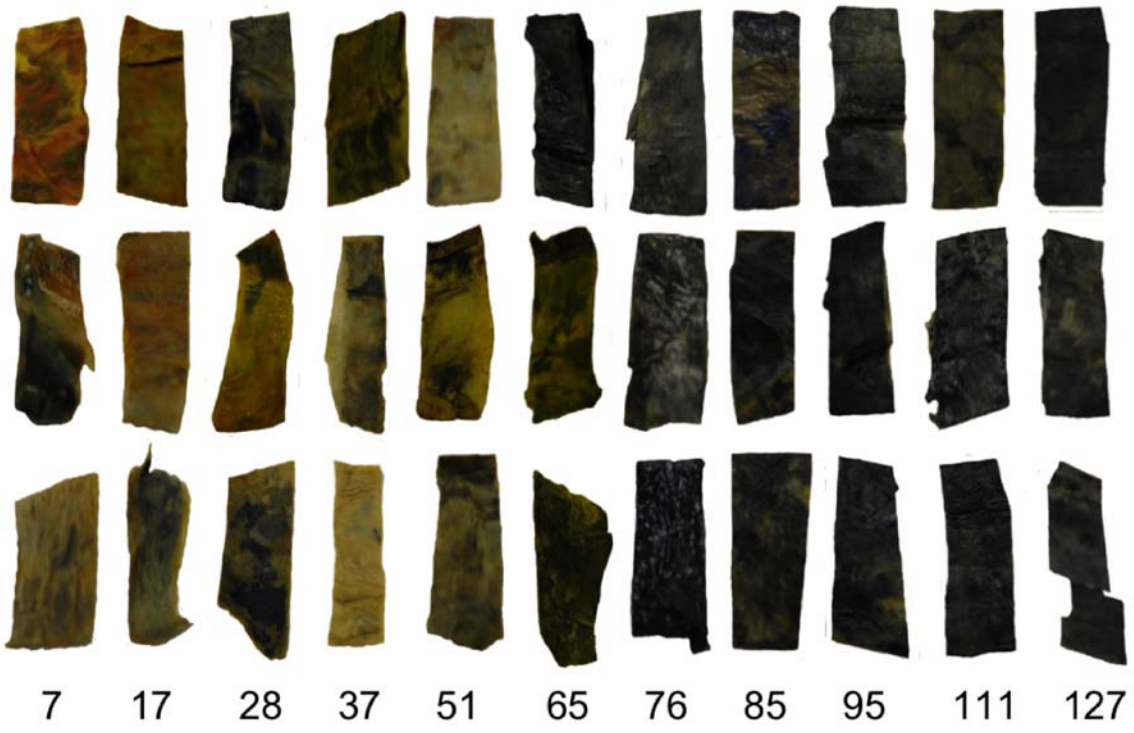

Figure 9: Visible pictures of *C. variopedatus* tubes over the incubation time-course.
(top) SdTUB treatment, (middle) PcTUB treatment, (bottom) LchTUB treatment. The numbers below the pictures indicate the time in days. Each tube piece is approximately 1 cm x 2 cm.

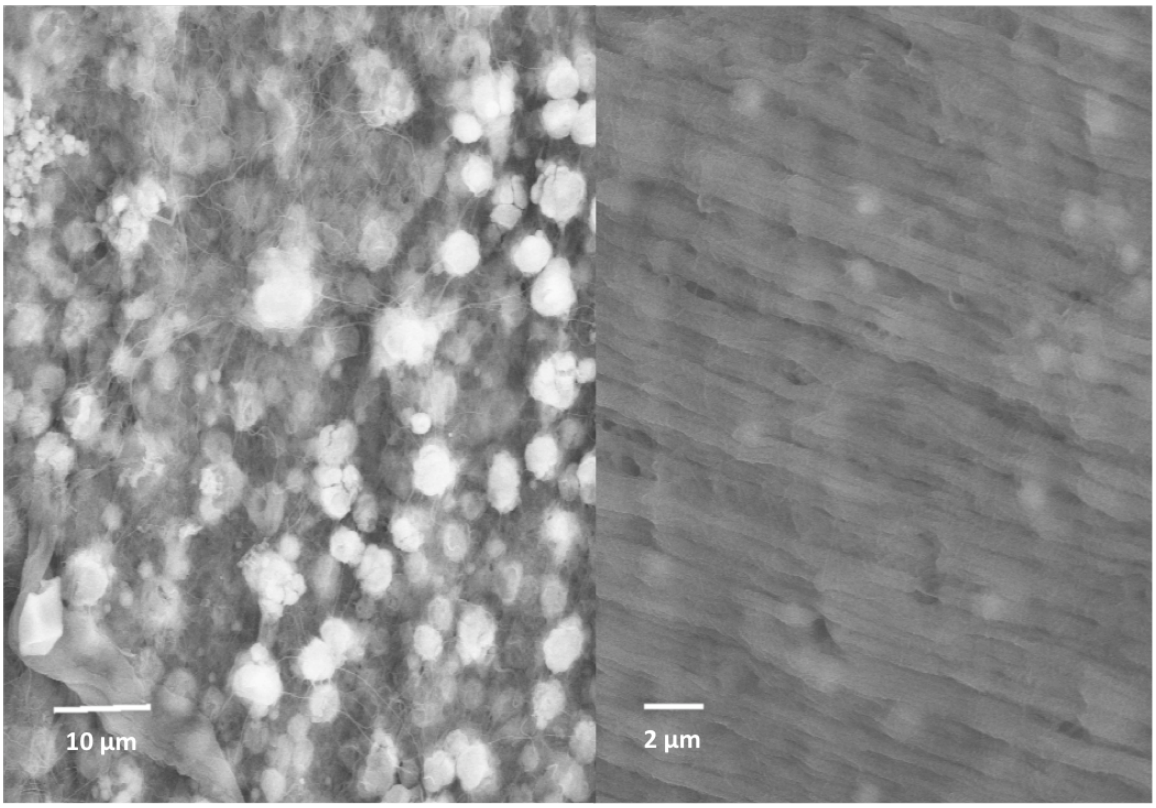

Figure 10: Structural changes in the tube wall surface over the incubation time-course. (left) un-incubated fresh tube, (right) incubated tube from day 85.

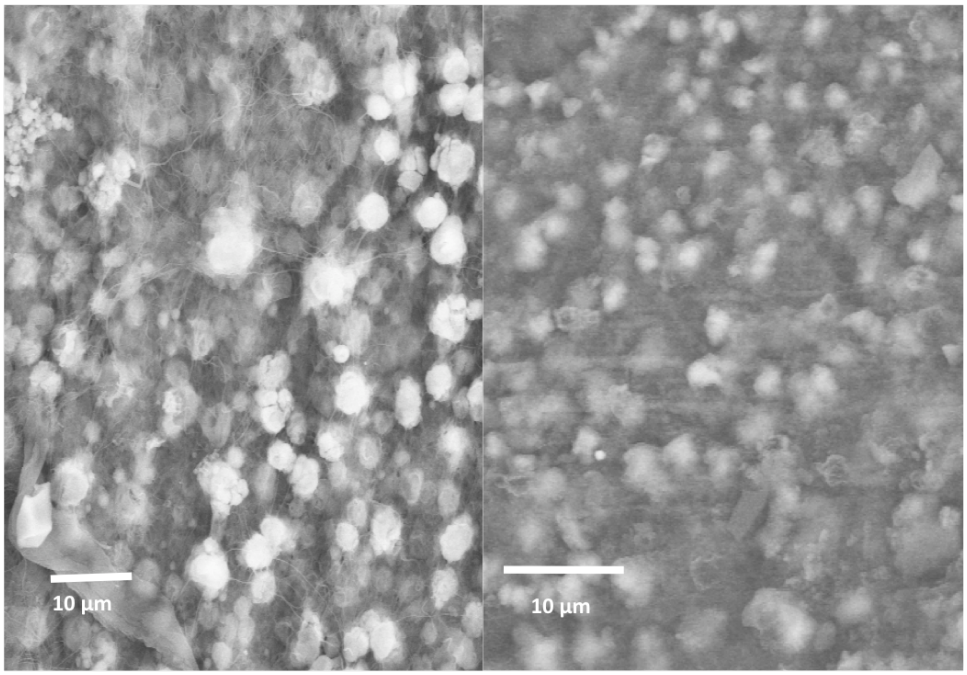

Figure 11: Changes in metal precipitates over the incubation time-course. (left) fresh un-incubated tube, precipitates are rich in Mn, Fe, Ca, P and O. (right) incubated tube from day 65, precipitates are rich in Fe and S.

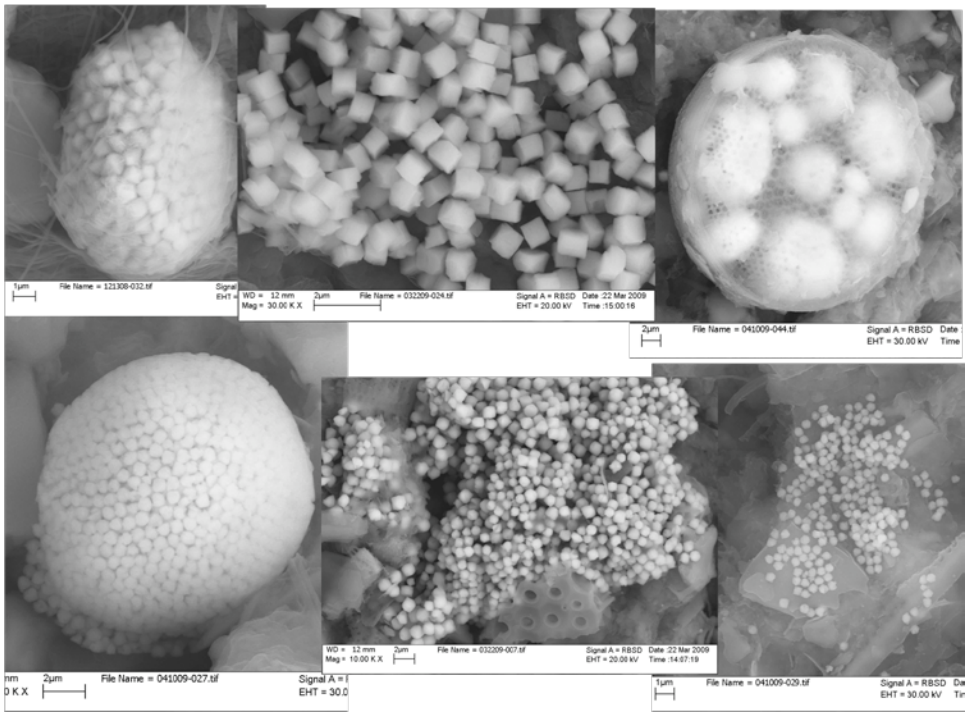

Figure 12: Framboids on the surfaces of incubated tubes. Diatoms such as the one illustrated top right act as centers of nucleation for these iron pyrites.

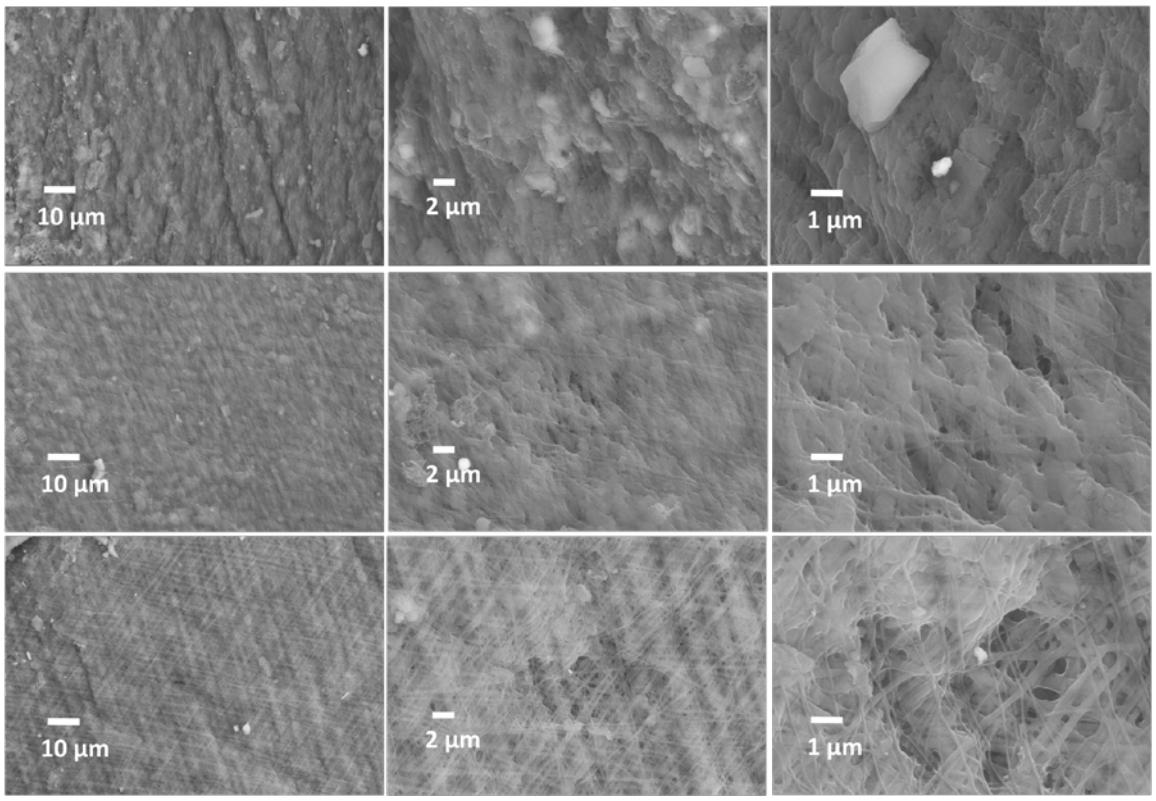

Figure 13: Examination of different layers of tube lining from SedTUB treatment at day 28. (top) outermost layer has lost the most structural integrity in the mesh matrix, (middle) one layer down the mesh structure is more intact, (bottom) one more layer down the fibrous matrix still has considerable structural integrity.

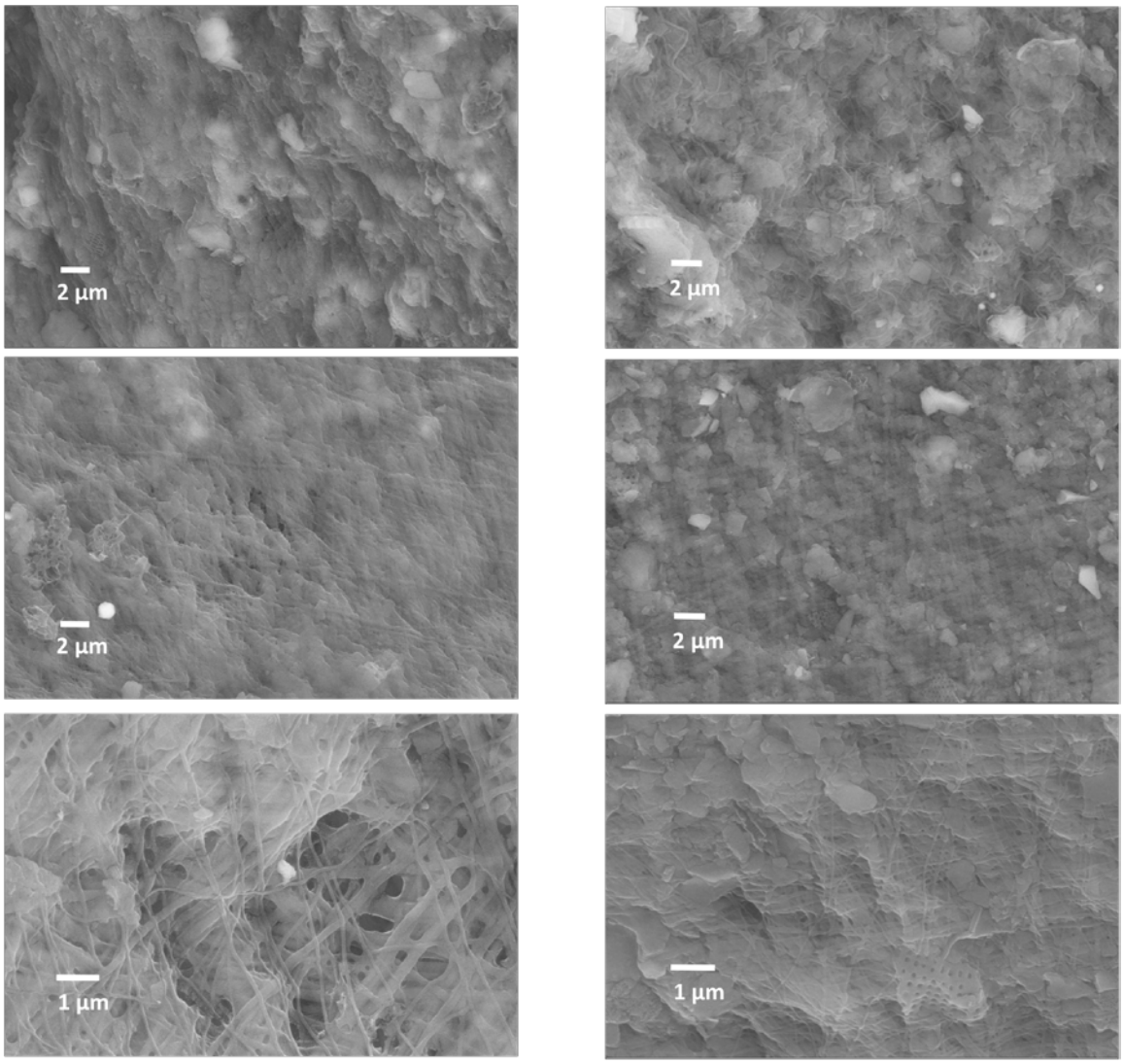

Figure 14: Comparison of different layers of tube lining from (left) SedTUB and (right) PcTUB treatments at day 28. PcTUB tube ends are more exposed and appear to have lost more structural integrity.

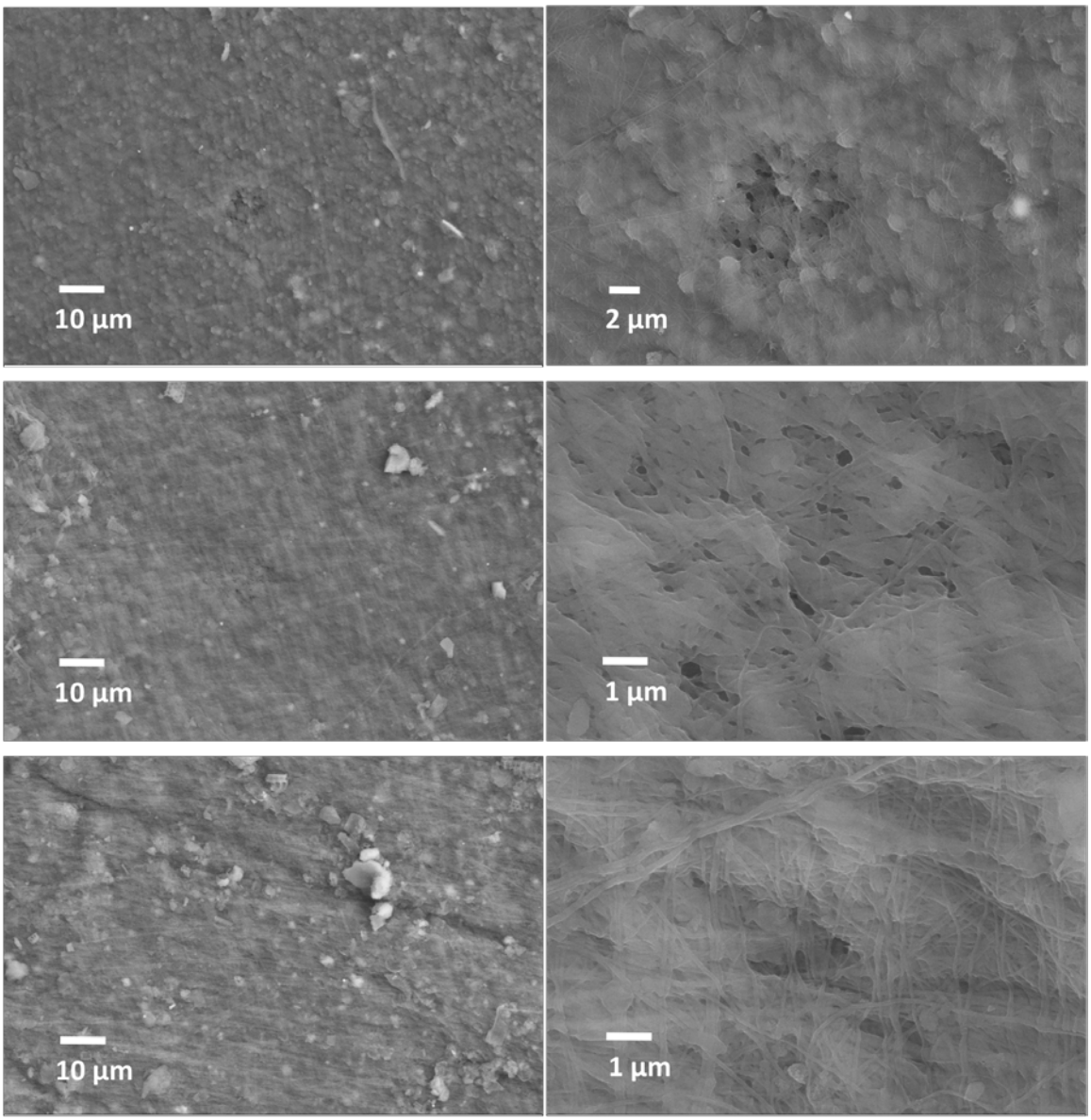

Figure 15: Examination of different layers of tube lining from SedTUB treatment at day 65. (top) outermost layer has lost the most structural integrity, (middle) one layer down the mesh structure is losing structural integrity, (bottom) one more layer down the mesh is also starting to lose structural integrity and the fibrous structure is quite amorphous when compared to similar pictures at day 28 (lower left column in Figure 13).

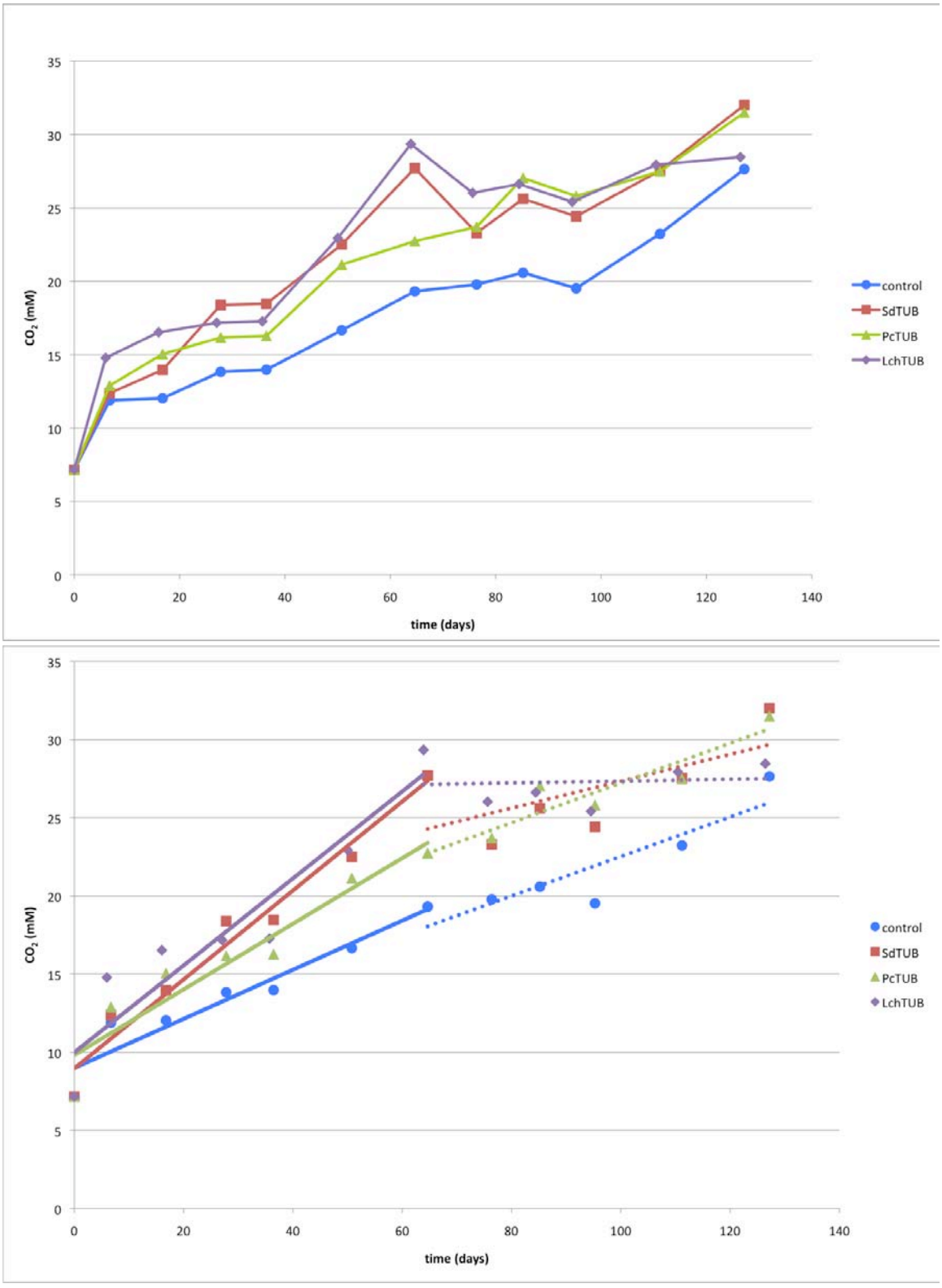

Figure 16: (top) TCO_2 production over the incubation time course. (bottom) CO_2 production is analyzed in two segments; (—) day 0-64 linear trendline, (····) day 64-125 linear trendline.

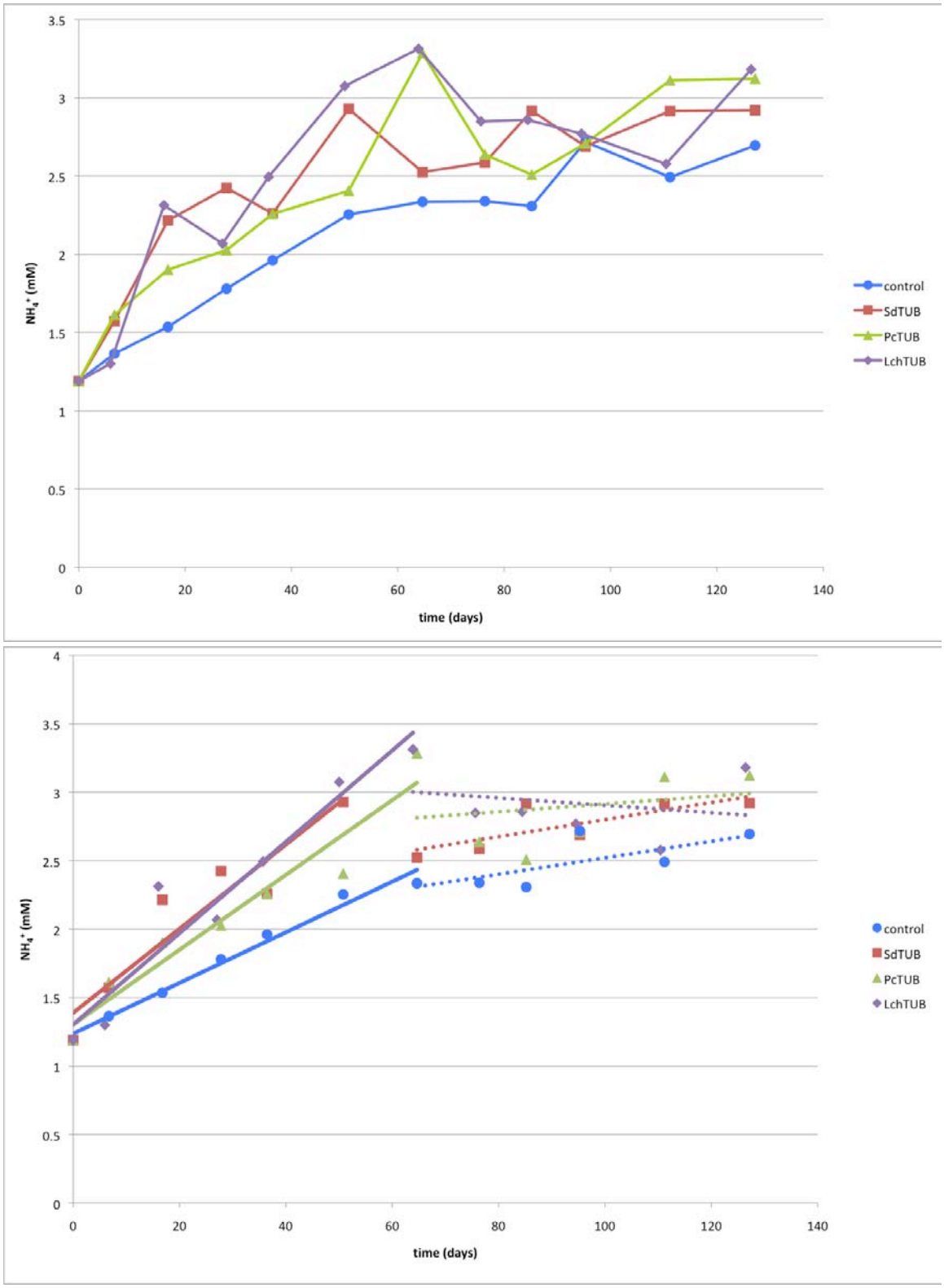

Figure 17: (top) NH_4 production over the incubation time course. (bottom) NH_4 production is analyzed in two segments; (—) day 0-64 linear trendline (0-51 for SdTUB), (····) day 64-125 linear trendline.

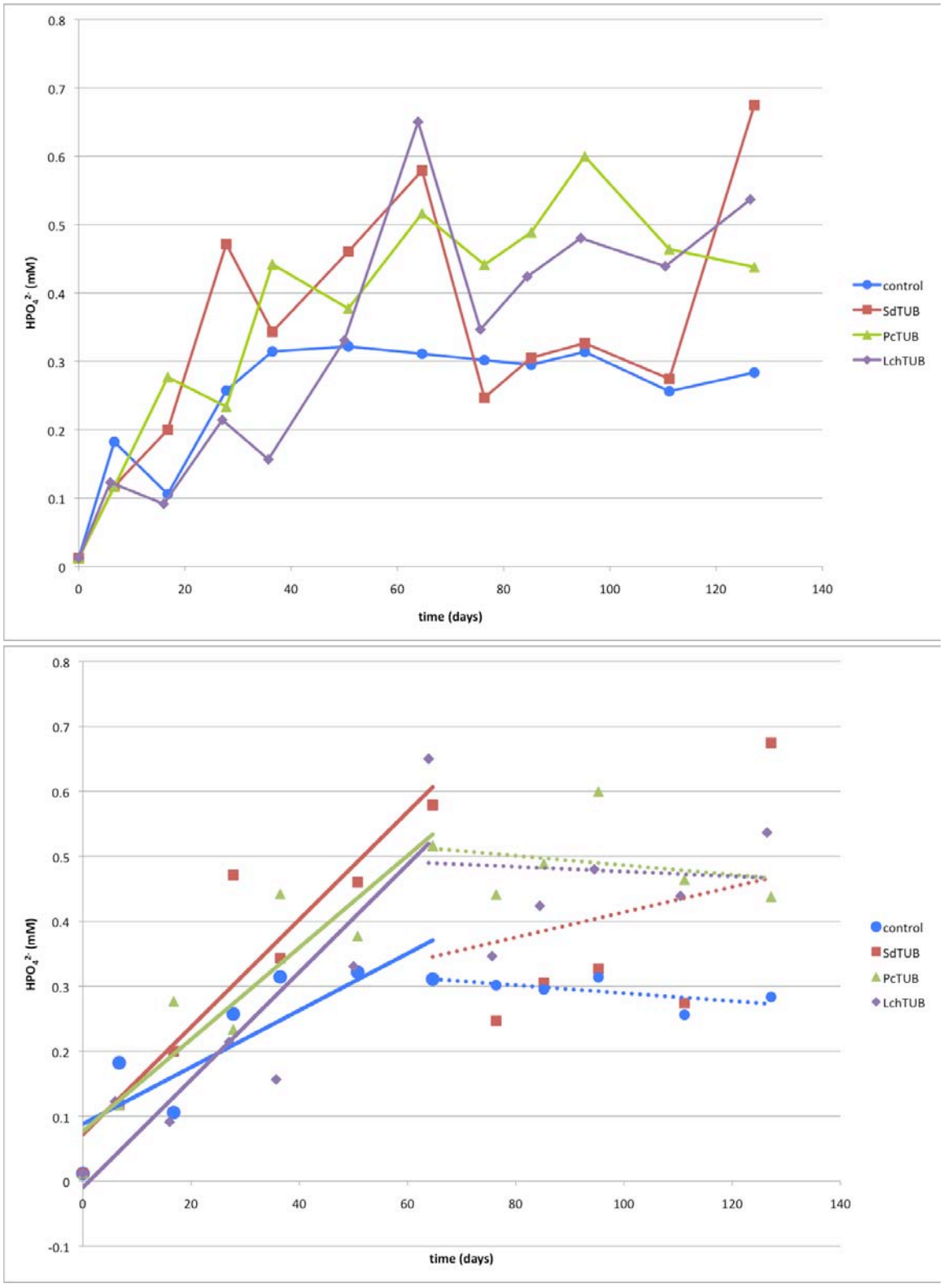

Figure 18: (top) HPO_4^{2-} production over the incubation time course. (bottom) HPO_4^{2-} production is analyzed in two segments; (—) day 0-64 linear trendline, (····) day 64-125 linear trendline.

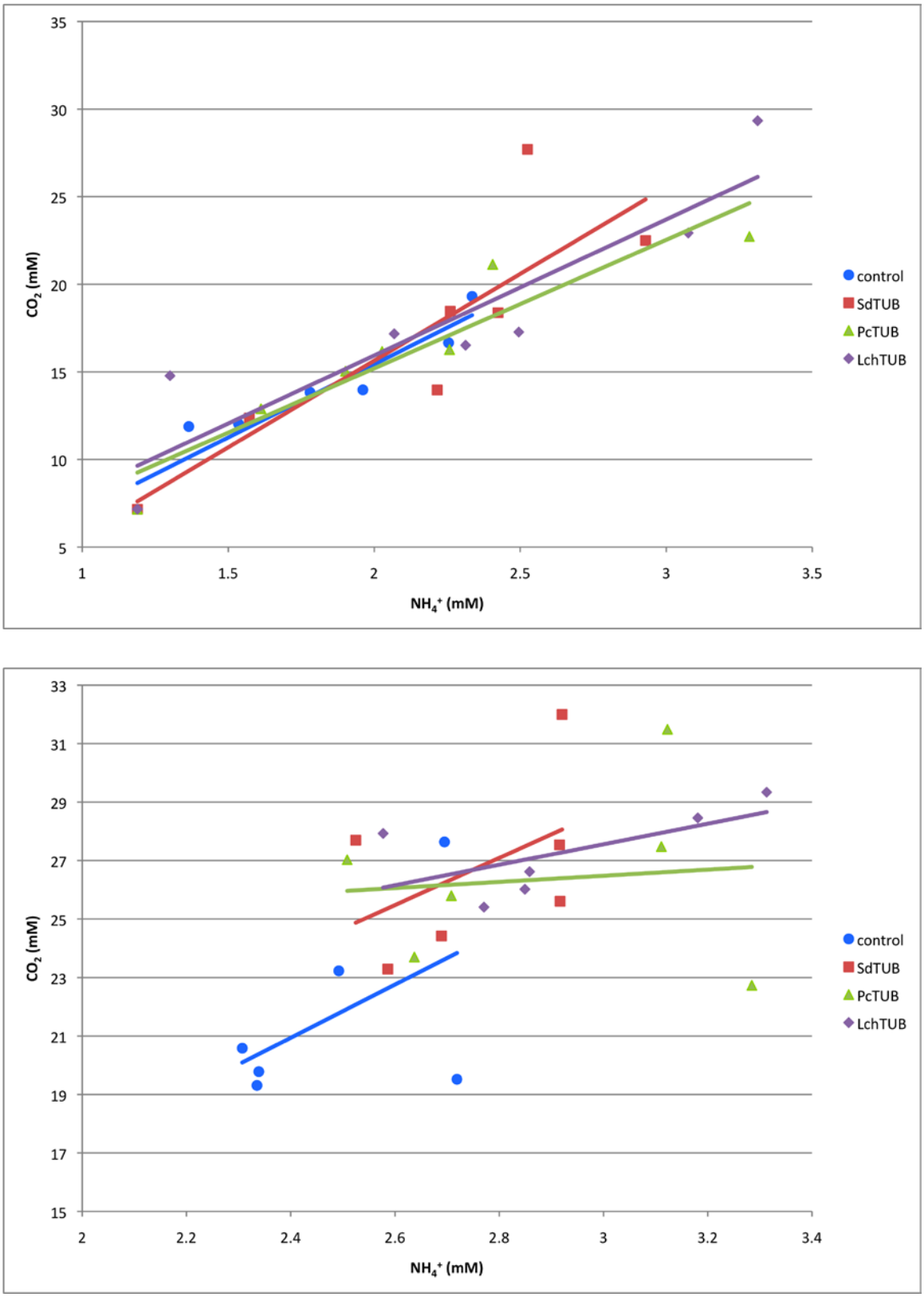

Figure 19: C:N production over the incubation time course. (top) 0-64 days, (bottom) 64-125 days.

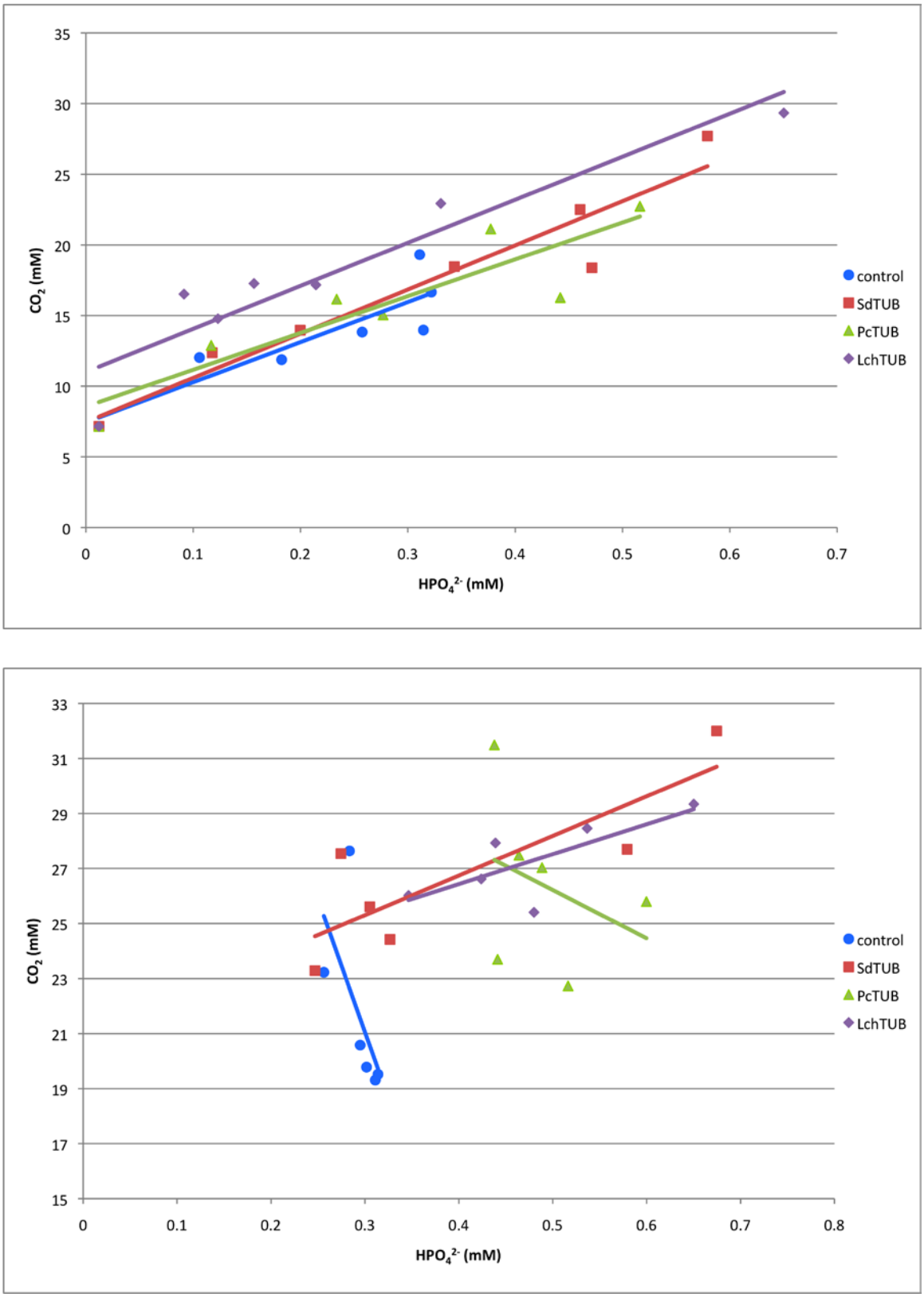

Figure 20: C:P production over the incubation time course. (top) 0-64 days, (bottom) 64-125 days.

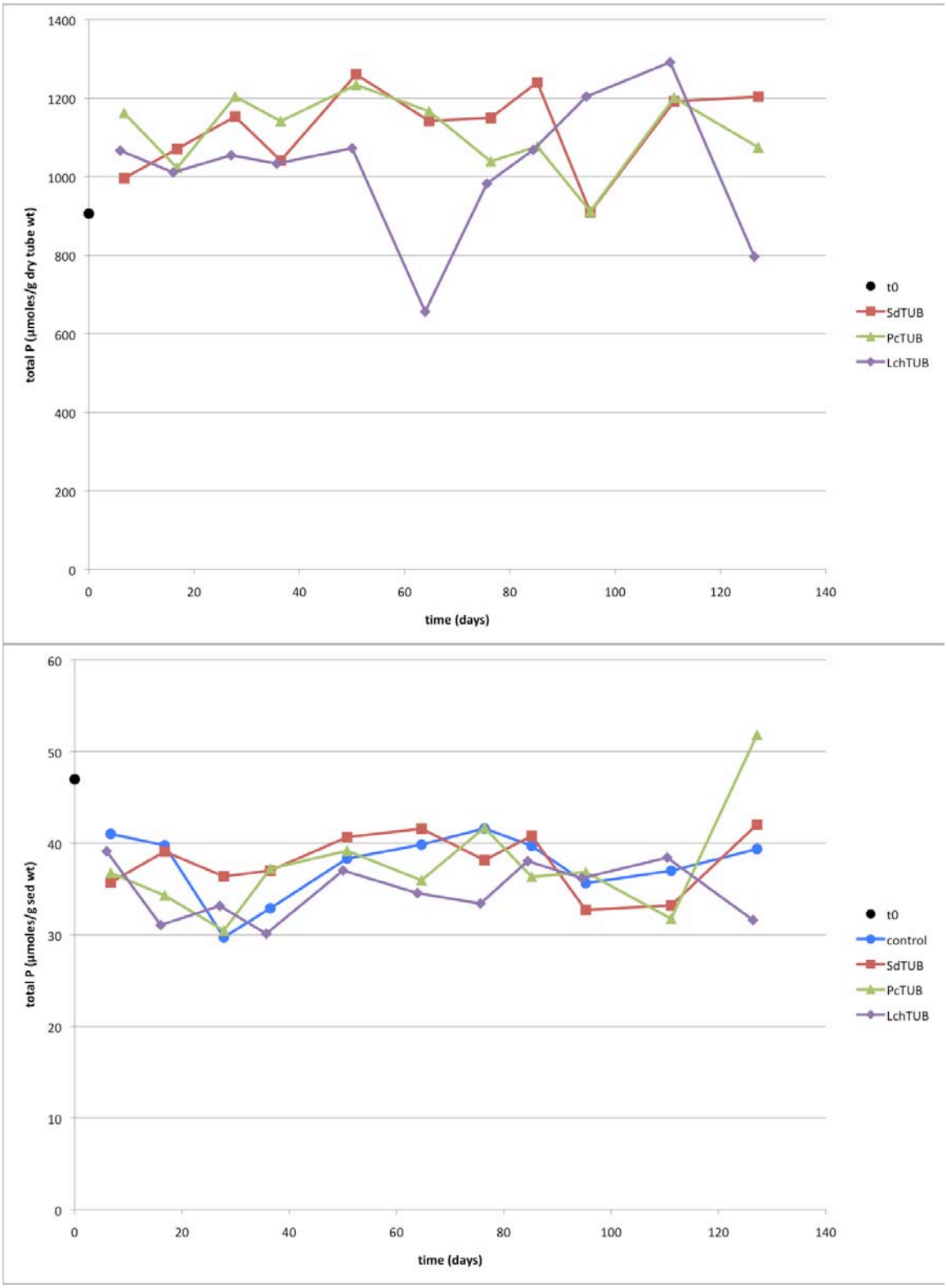

Figure 21: Total solid phosphorus in tubes (top) and sediments (bottom).

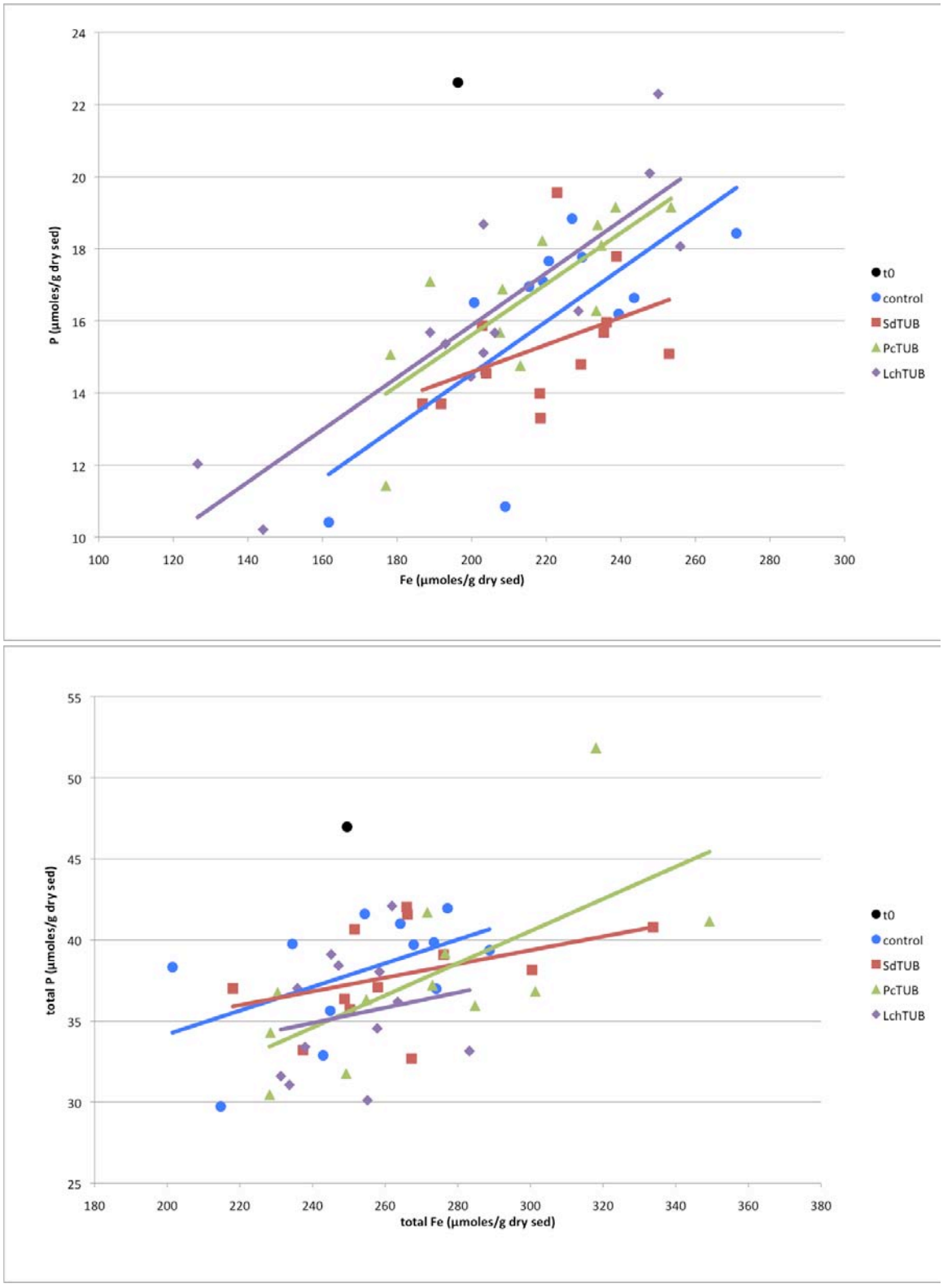

Figure 22: Solid P vs Fe for sediments; (top) inorganic pool (defined as more easily accessible pool for Fe), (bottom) total pool.

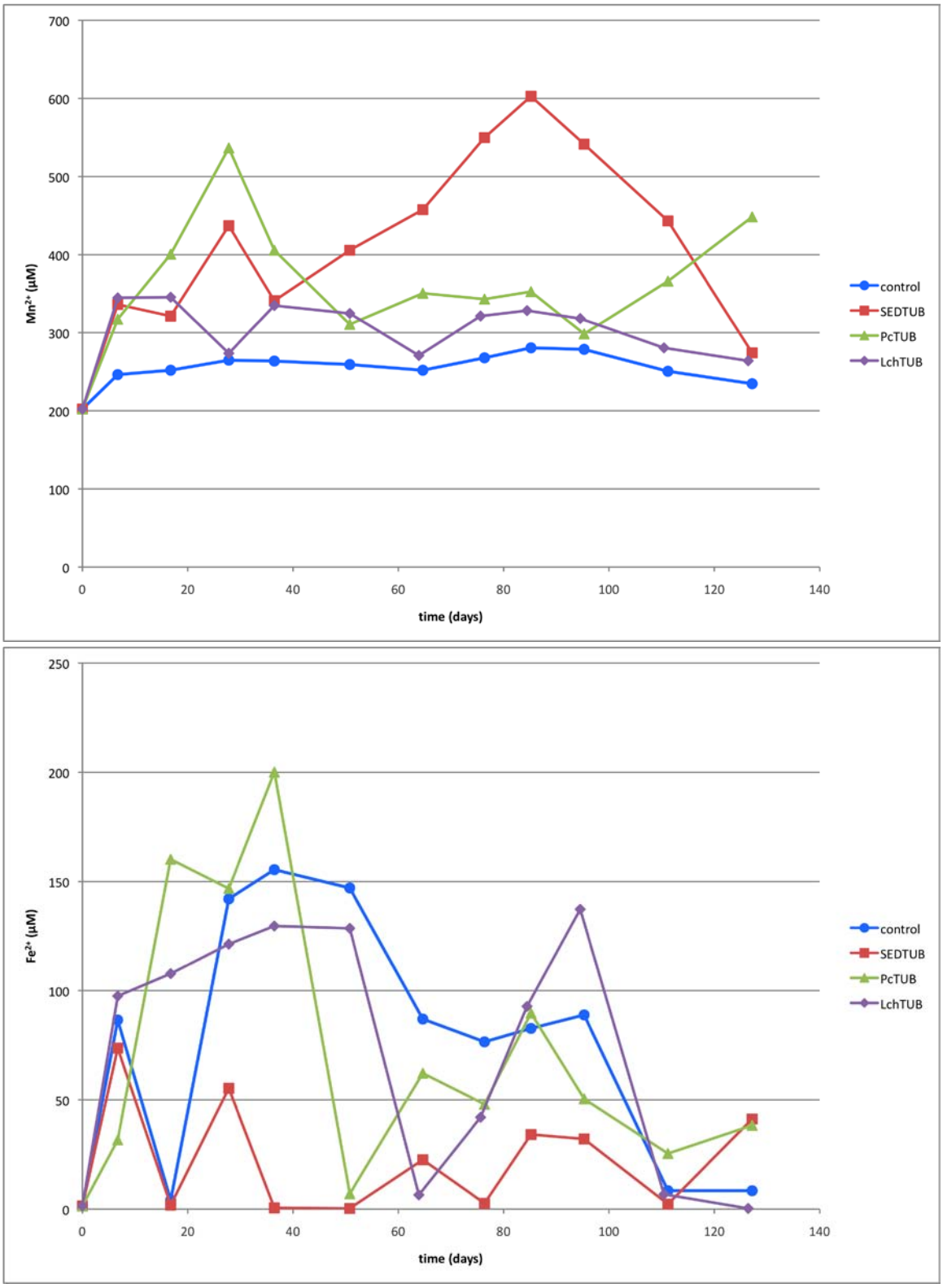

Figure 23: Porewater Mn^{2+} (top) and Fe^{2+} (bottom) over the incubation time course.

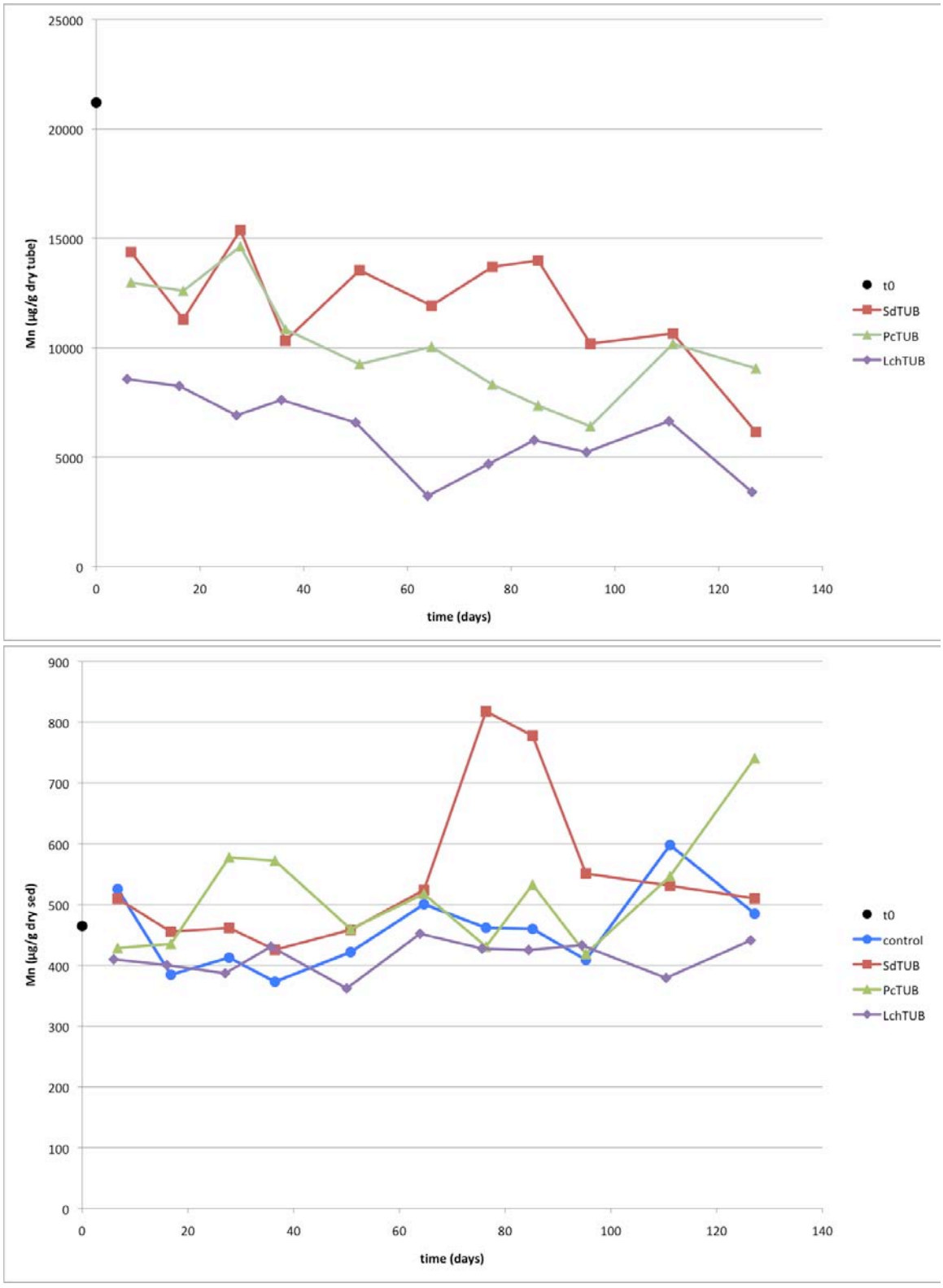

Figure 24: Total solid phase Mn in tubes (top) and sediments (bottom) over the incubation time course.

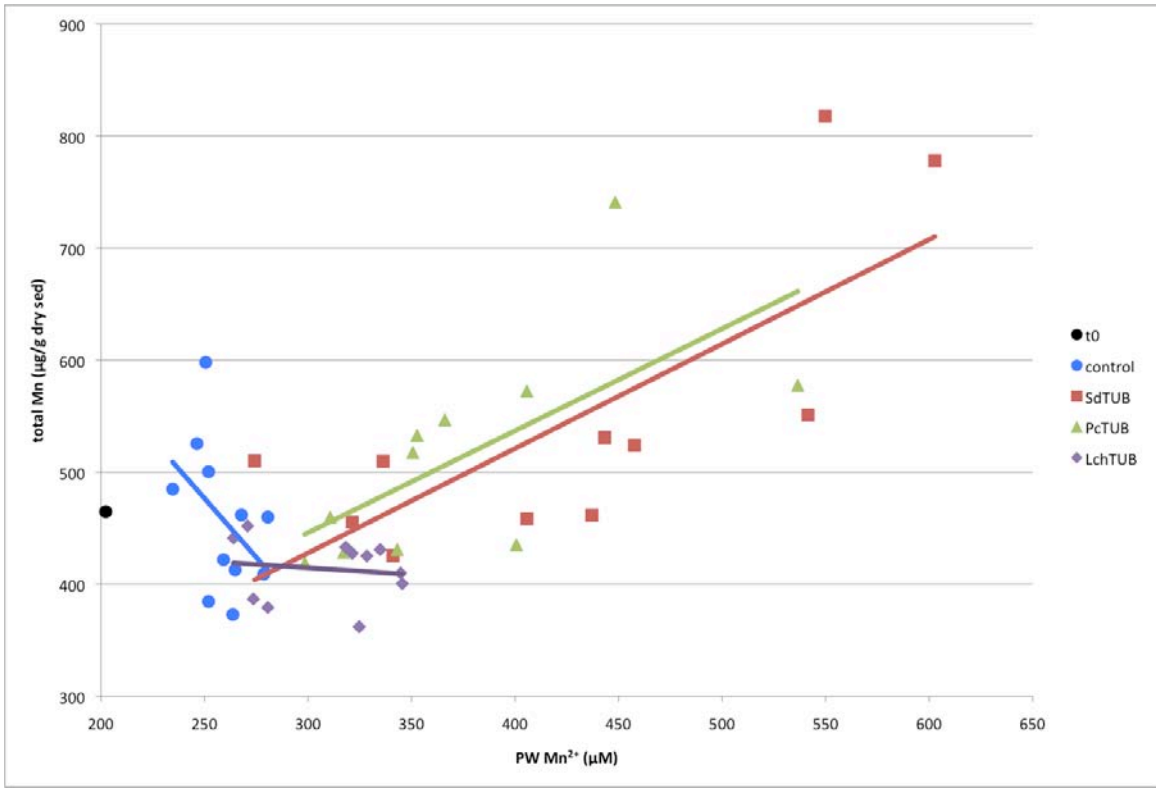

Figure 25: Total solid Mn in sediments vs porewater Mn^{2+}.

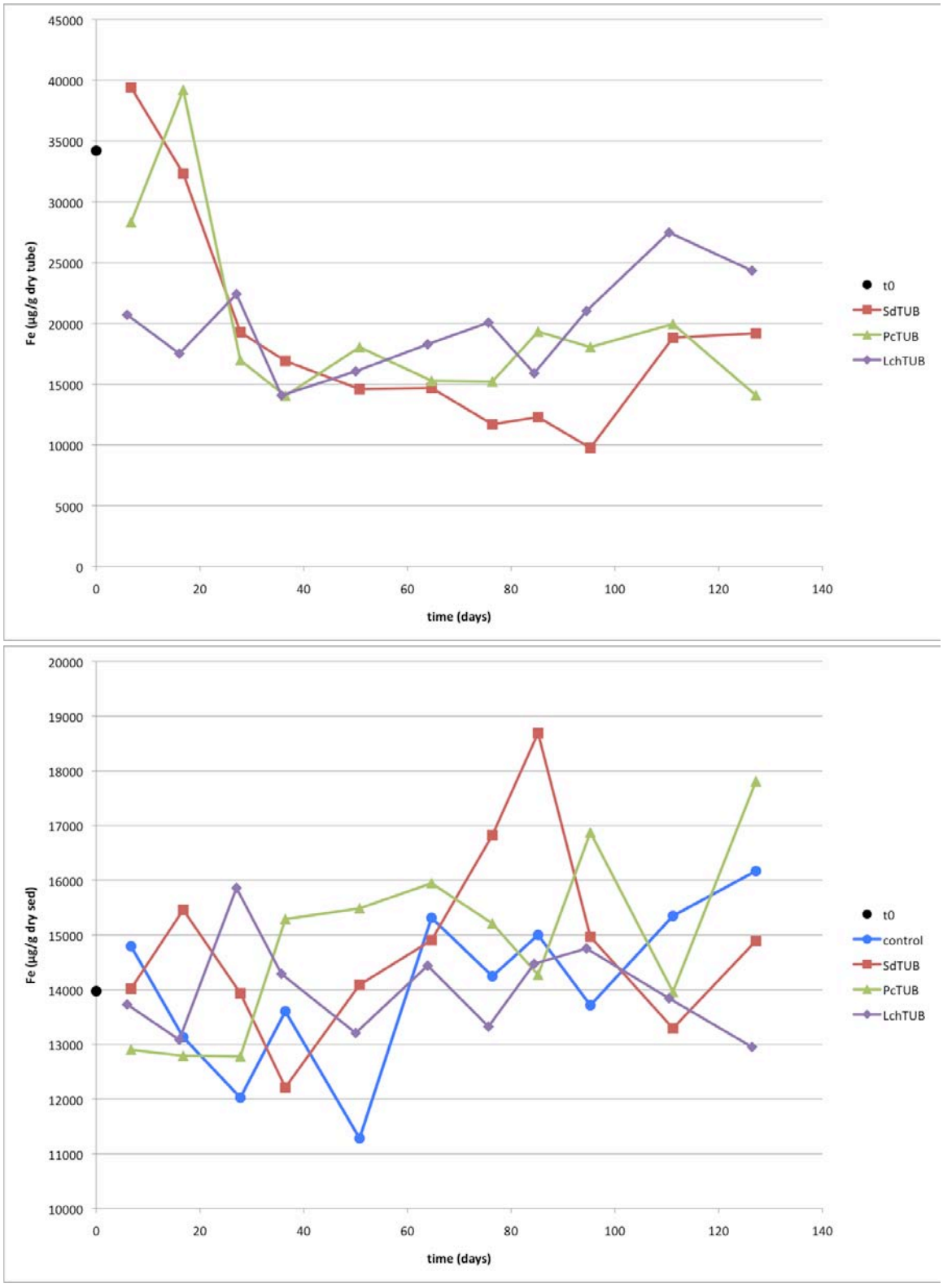

Figure 26: Total solid phase Fe in tubes (top) and sediments (bottom) over the incubation time course.

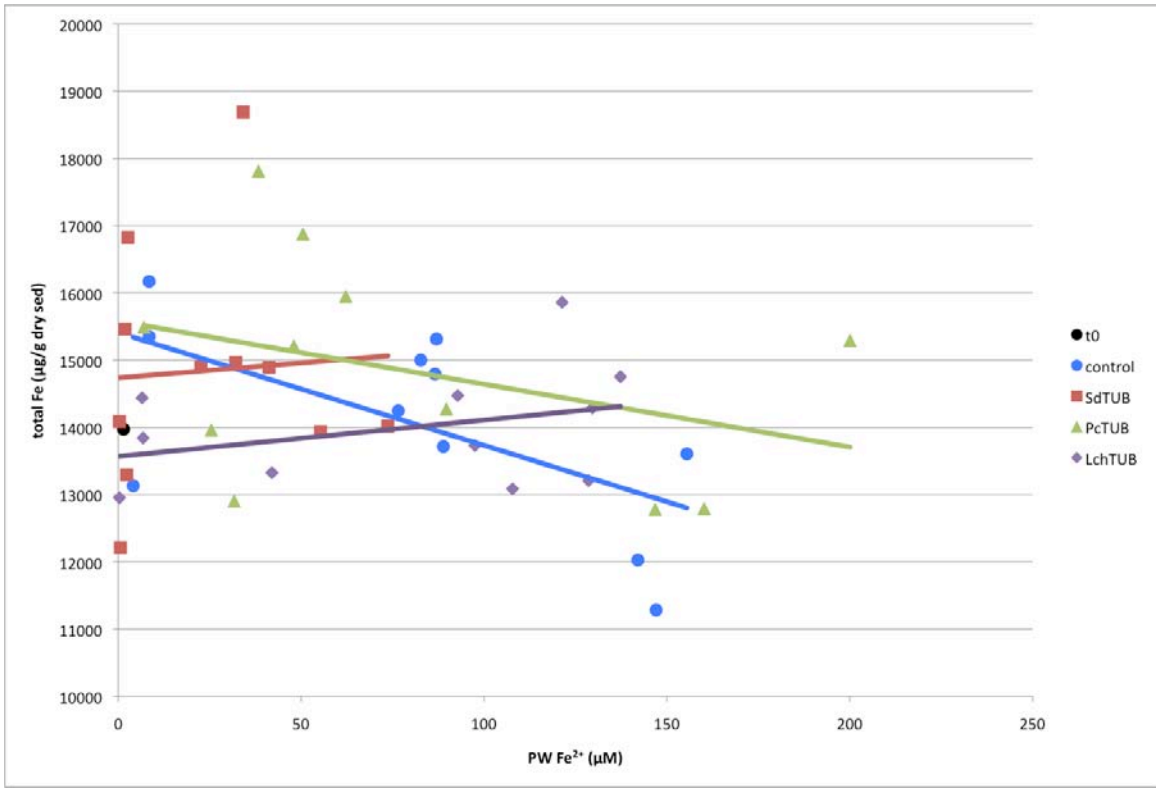

Figure 27: Total solid Fe in sediments vs porewater Fe^{2+}.

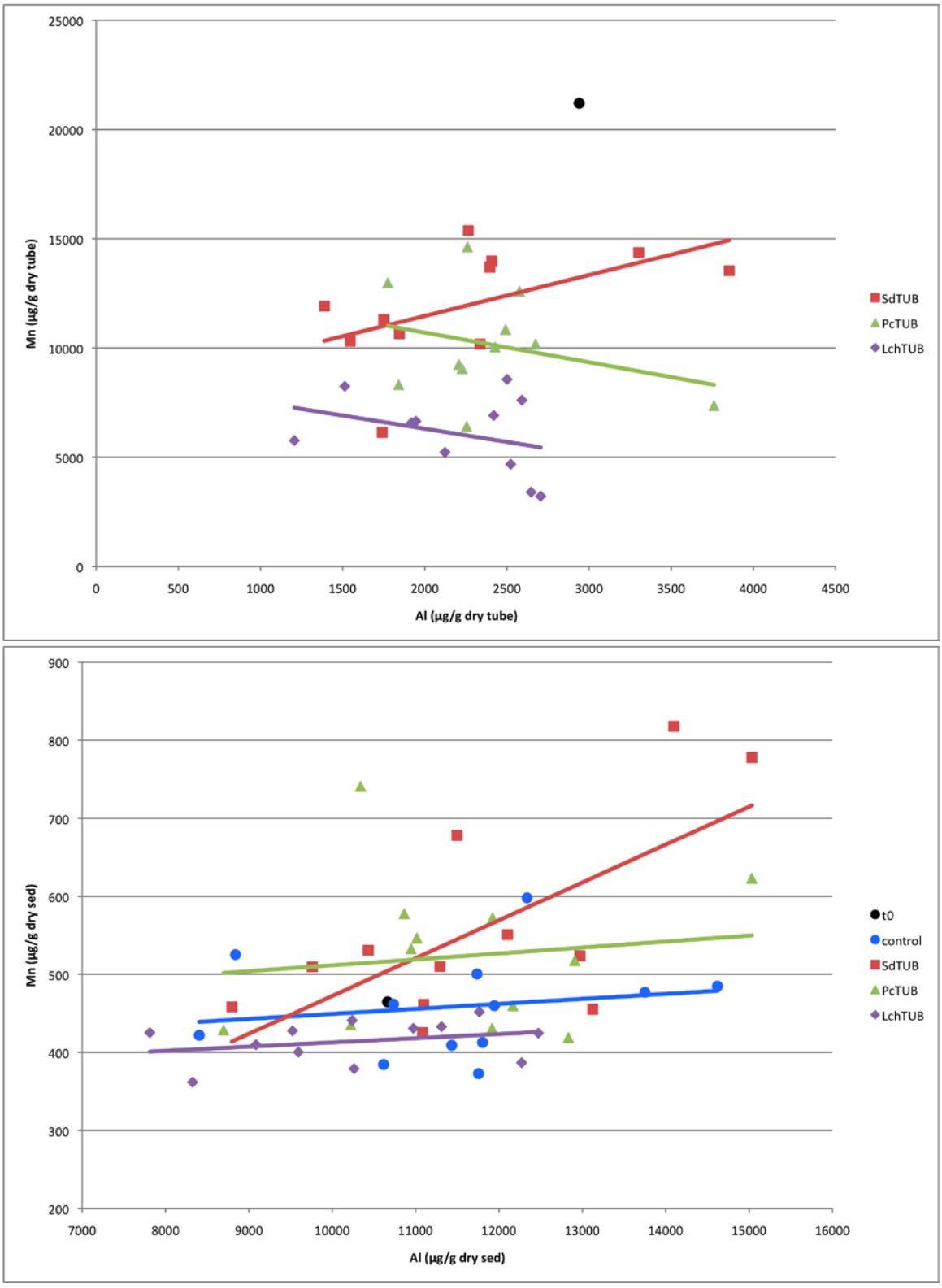

Figure 28: Total solid Mn vs total solid Al in tubes (top) and sediments (bottom).

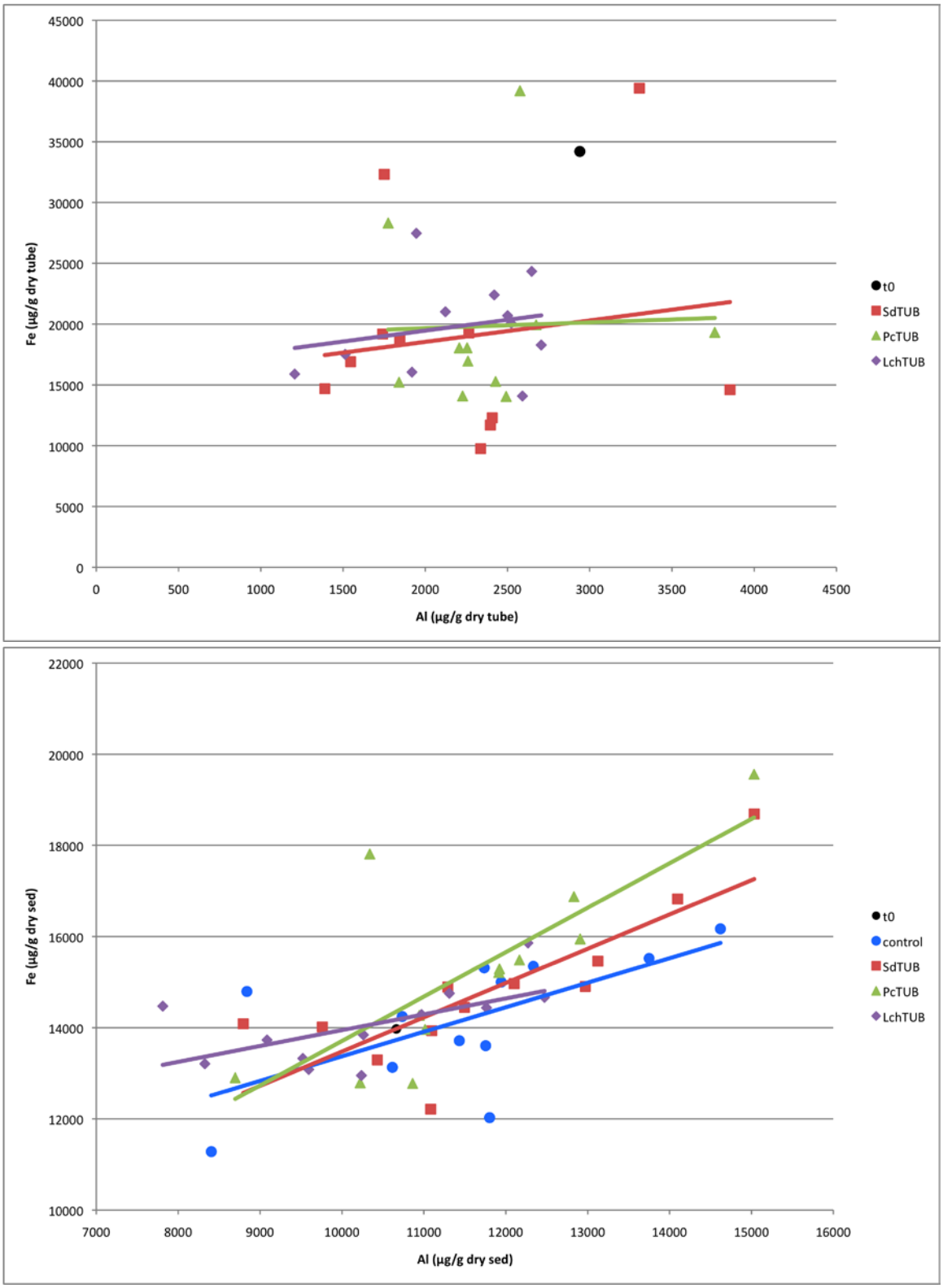

Figure 29: Total solid Fe vs total solid Al in tubes (top) and sediments (bottom).

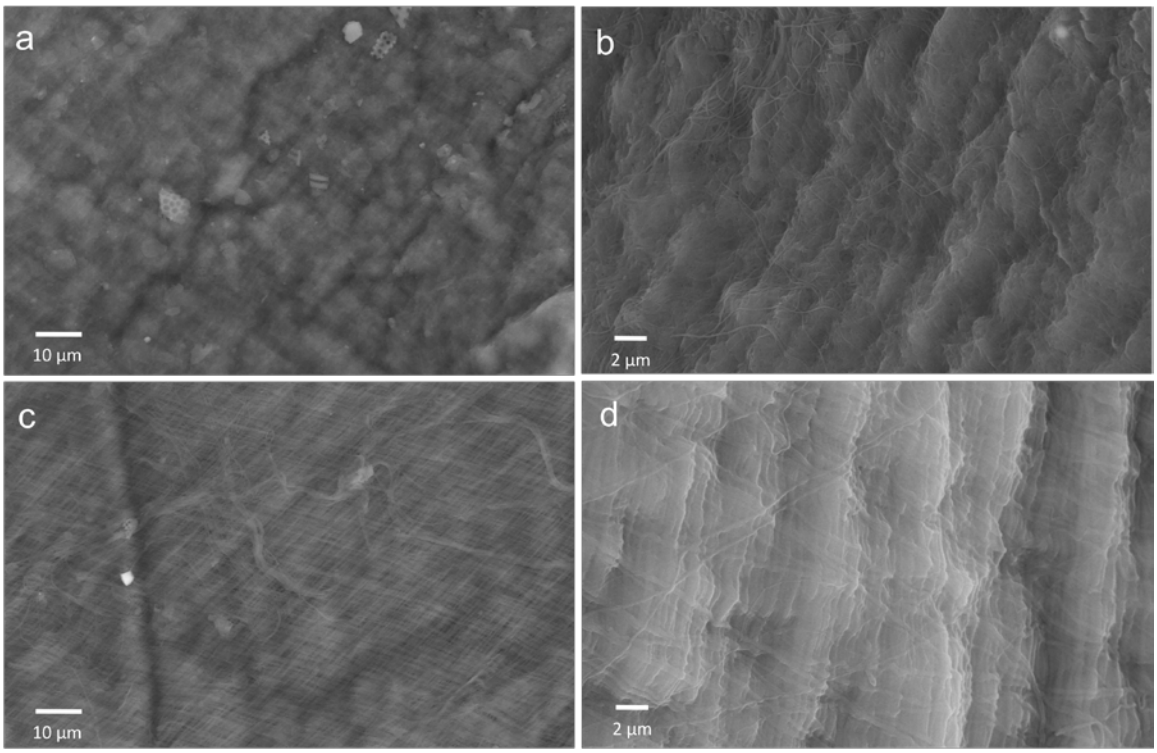

Figure 30: SEM pictures of other tube linings. (a) Axiothellae, (b) Diopatra, (c) Onuphis, (d) Chaetopterus. All tubes were collected in South Carolina.

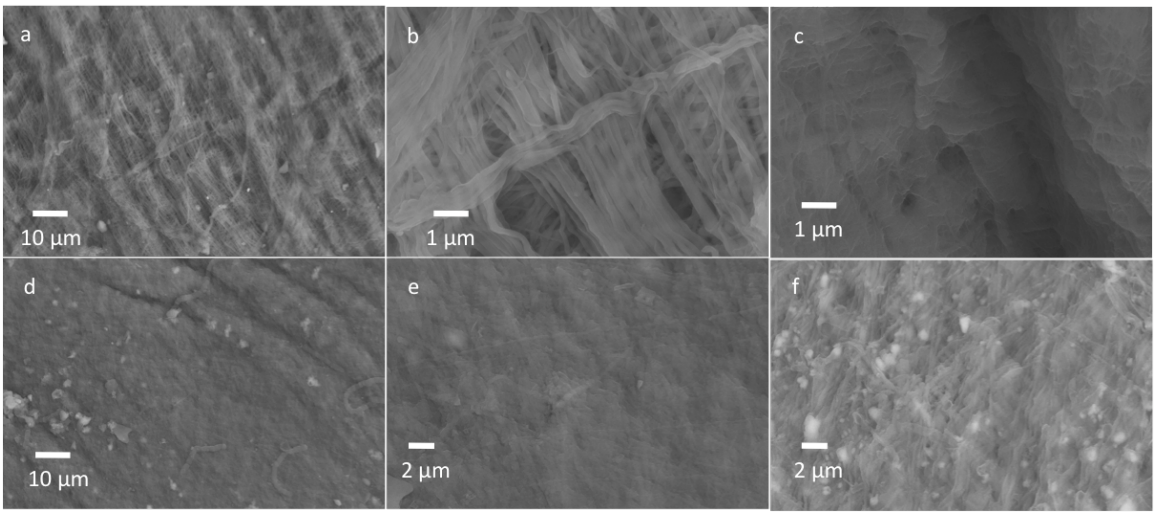

Figure 31: SEM pictures of tubes in LchTUB treatment. (a) & (b) day 7, (c) day 37, (d) & (e) day 65, (f) day 85.

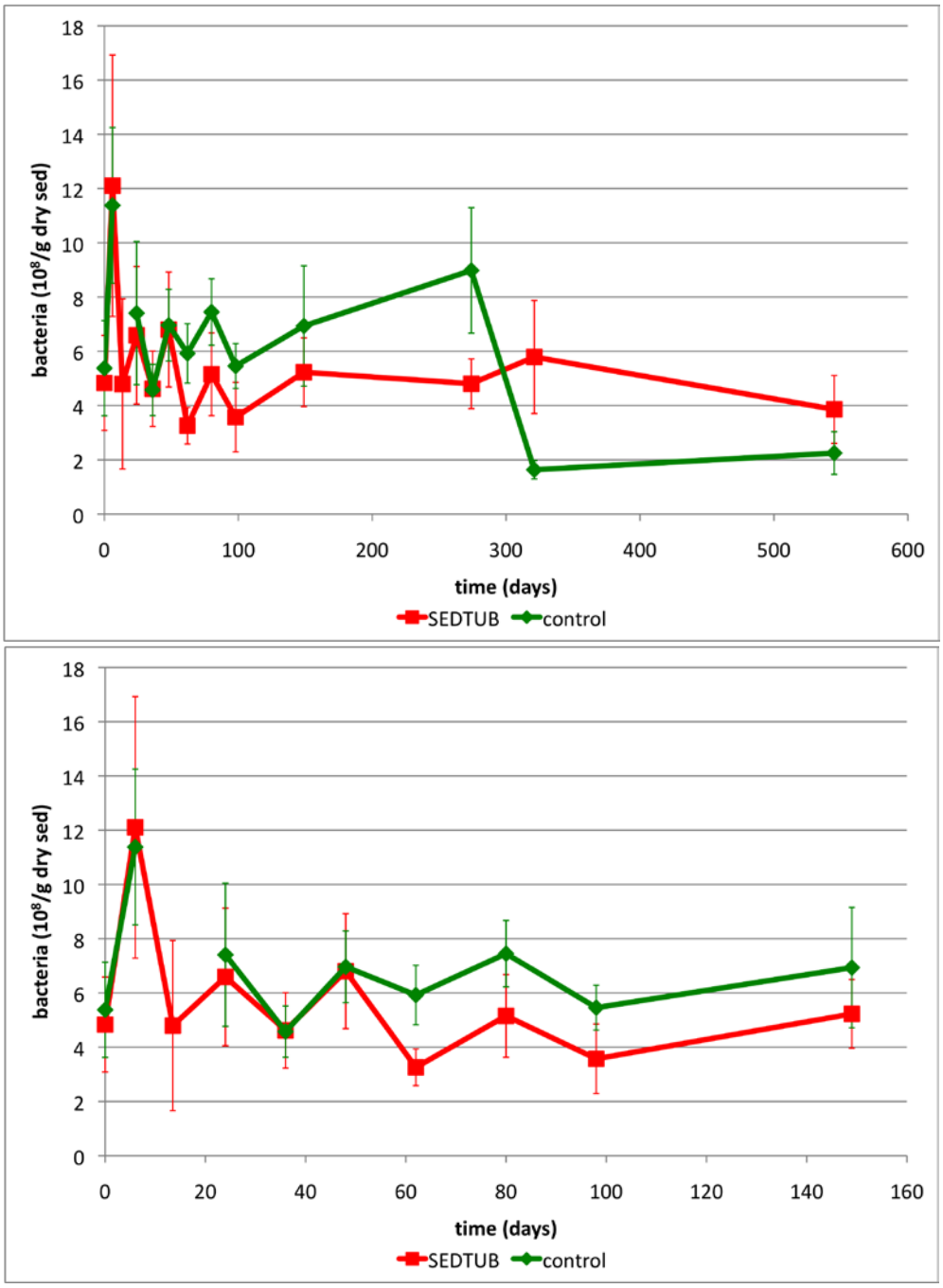

Figure 32: Counts of total sediment bacteria from a set of anoxic sediment incubations with *C. variopedatus* tubes. (top) 0-550 days, (bottom) same data set, 0-149 days. The control sample at day 17 was contaminated and was not included in these graphs. SEDTUB = tubes in anoxic sediment, control = anoxic sediment without tubes.

Macrofaunal Process	Effect	Decomposition rate/extent
Particle manipulation	Substrate exposure; increase of surface area	+
Grazing, digestion	Bacterial growth stimulation, enzymes released, redox oscillation	+
Excretion, secretion	Mucus substrate, Nutrient release, bacterial growth stimulation	+
Construction, secretion	Synthesis of refractory structural products, e.g. tube linings	-
Irrigation	Soluble reactants supplied, metabolite build-up lowered, increased reoxidation, redox oscillation	+
Particle transport	Transfer between major redox zones, increased reoxidation, redox oscillation	+

Table 1: Macrofaunal effects on organic matter decomposition and remineralization in sediments (Aller, 2001).

Sample	% C	% N	% P	C:N	C:P
Chaetopterus variopedatus, Long Island Sound[a]	22.7	3.56	5.21	7.43	11.3
Chaetopterus variopedatus, South Carolina[a]	17.8	2.34	4.24	8.87	10.8
Axiothella, South Carolina[a]	16.8	b.d.	3.70	-	11.7
Diopatra, South Carolina[a]	9.12	0.557	3.77	19.1	6.25
Onuphis, South Carolina[a]	7.82	b.d.	1.48	-	13.6
Long Island Sound sediment[a]	2.2	0.4	0.12	6.42	47.4
Fresh phytoplankton[b]				6.7	106

Table 2: Elemental concentrations in *Chaetopterus variopedatus* and other tube linings. [a]this study, [a]Redfield et al, 1963.

Amino acid	**Composition of fresh tube (mol %)**	**Composition of tube incubated in anoxic sediment for 112 days (mol %)**
ASP	9.56	10.1
GLU	5.59	6.32
SER	3.01	3.33
HIS	0.62	0.75
Glucosamine	33.1	22.5
GLY	7.94	7.69
THR	4.30	4.24
ARG	1.87	2.15
BALA	14.6	8.74
ALA	3.33	3.92
GABA	0.66	0.57
TYR	0.77	1.11
MET	0.15	0.01
VAL	3.96	3.52
PHE	1.52	2.18
ILE	2.66	2.62
LEU	2.96	3.03
LYS	3.11	2.93

Table 3: Amino acid composition of *Chaetopterus variopedatus* tube linings.

Treatment	ΣCO_2 (mmol/ m^2-d)	p value/ R^2	NH_4^+ (mmol/ m^2-d)	p value/ R^2	HPO_4^{2-} (mmol/ m^2-d)	p value/ R^2
Control	5.73	<0.001/0.93	0.783	<0.001/0.97	0.145	0.06/0.55
SdTUB	10.7	<0.001/0.91	0.722 (1.14)	0.06 (0.03)/ 0.53 (0.78)	0.326	0.01/0.76
PcTUB	7.52	<0.001/0.94	1.13	<0.001/0.88	0.268	0.02/0.76
LchTUB	10.5	0.01/0.84	1.40	0.01/0.86	0.378	0.02/0.73

Table 4: Production estimates of C, N and P from day 0 to day 64. The numbers in parentheses for SdTUB represent a linear regression fit from day 0 to day 51. p values are reported at the 90% confidence level.

Treatment	ΣCO_2 (mmol/ m^2-d)	p value/ R^2	NH_4^+ (mmol/ m^2-d)	p value/ R^2	HPO_4^{2-} (mmol/ m^2-d)	p value/ R^2
Control	6.71	0.03/0.78	0.290	0.19/0.31	-0.0264	0.32/0.10
SdTUB	6.90	0.02/0.83	0.224	0.23/0.24	0.299	0.11/0.49
PcTUB	5.60	0.03/0.76	0.554	0.03/0.77	-0.0264	0.75/-0.28
LchTUB	2.27	0.09/0.57	0.163	0.56/-0.17	0.132	0.07/0.64

Table 5: Production estimates of C, N and P from day 64 to day 125. p values are reported at the 90% confidence level.

Treatment	Observed C:N	p value/R^2	Observed C:P	p value/R^2
Control	7.00	0.01/0.85	24.5	0.09/0.45
SdTUB	9.39 (7.61)	0.09 (0.03)/ 0.45 (0.80)	29.7	0.01/0.84
PcTUB	6.02	0.01/0.81	21.0	0.05/0.58
LchTUB	6.60	0.02/0.70	25.6	<0.001/0.94

Table 6: Observed C:N and C:P values for incubation treatments from day 0 to day 64. The numbers in parentheses for SdTUB represent a linear regression fit from day 0 to day 51. p values are reported at the 90% confidence level.

Treatment	Geometric mean slope of total Fe vs P	p value	Geometric mean slope of inorganic* Fe vs P	p value
Control	3.75	0.11	7.09	0.01
SdTUB	3.78	0.24	4.81	0.19
PcTUB	4.45	0.02	8.55	<0.001
LchTUB	1.08	0.46	10.4	<0.001

Table 7: Summary of solid Fe vs P in sediments. (*inorganic here refers to the less easily accessible pool.) p values are reported at the 90% confidence level.

Treatment	Geometric mean slope of solid Mn vs PW Mn^{2+}	p value	Geometric mean slope of solid Fe vs PW Fe^{2+}	p value
Control	-3.83	0.42	-8.25	0.58
SdTUB	0.448	0.15	3.86	0.91
PcTUB	0.469	0.26	-10.0	0.38
LchTUB	-0.268	0.67	-1.96	0.88

Table 8: Summary of solid Mn in sediments vs porewater Mn^{2+} & solid Fe in sediments vs porewater Fe^{2+}. p values are reported at the 90% confidence level.

Treatment	Geometric mean slope of total solid Mn vs Al in sediments	p value	Geometric mean slope of total solid Mn vs Al in tubes	p value
Control	0.0156	0.23		
SdTUB	0.0520	0.02	1.78	0.14
PcTUB	-0.004	0.87	-0.608	0.72
LchTUB	0.0055	0.38	-1.30	0.21

Table 9: Summary of solid Mn vs Al in sediments and tubes. p values are reported at the 90% confidence level.

Treatment	Geometric mean slope of total solid Fe vs Al in sediments	p value	Geometric mean slope of total solid Fe vs Al in tubes	p value
Control	0.765	<0.001		
SdTUB	0.803	<0.001	-2.97	0.32
PcTUB	1.05	0.01	2.74	0.59
LchTUB	0.354	0.05	2.46	0.37

Table 10: Summary of solid Fe vs Al in sediments and tubes. p values are reported at the 90% confidence level.

REFERENCES

Aller, R. C. 1982. The effects of macrobenthos on chemical properties of marine sediment and overlying water *in* Animal-Sediment Relations, P. L. McCall and P. J. S. Tevesz, eds., Plenum, New York, 53-102.

Aller, R. C. 1983. The importance of the diffusive permeability of animal burrow linings in determining marine sediment chemistry. *J. Mar. Res.* 41: 299-322.

Aller, R. C. 1988. Benthic fauna and biogeochemical processes in marine sediments: The role of burrow structures *in* Nitrogen Cycling in Coastal Marine Environments, T. H. Blackburn and J. Sorensen, eds., John Wiley & Sons Ltd., 302-337.

Aller, R. C. 1994. Bioturbation and remineralization of sedimentary organic matter: effects of redox oscillation. *Chem. Geol.* 114: 331-345.

Arnosti, C., D. J. Repeta and N. V. Blough. 1994. Rapid bacterial degradation of polysaccharides in anoxic marine systems. *Geochim. Cosmochim. Acta* 58(12): 2639-2652.

Aspila, K.I., H. Agemian, and A.S.Y. Chau. 1976. A semi-automated method for the determination of inorganic, organic and total phosphate in sediments. *Analyst* 101: 187-197.

Berkeley, Cyril. 1922. On the occurrence of manganese in the tube and tissues of *Mesochaetopterus Taylori*, Potts, and in the tube of *Chaetopterus Variopedatus*, Renier. *Biochemical Journal* 16(1): 70-77.

Berner, R. A. 1977. Stoichiometric models for nutrient regeneration in anoxic sediments. *Limnol. Oceanogr.* 22(5): 781-786.

Berner, R. A. 1981. A rate model for organic matter decomposition during bacterial sulfate reduction in marine sediments. *Biogéochemie de la matière organique à l interface eau-sédiment marin.* Colloques Internationaux du C. N. R. S. no. 293.

Bishop, S. H., T. A. Bunde and G. E. Dearlove. 1978. Cerianthin: A silk-like protein from sea anemones. *Federation Proceedings* 37: 1528.

Brown, S. C. and S. McGee-Russell. 1970. *Chaetopterus* tubes: Ultrastructural architecture. *Tissue Cell* 3(1): 65-70.

Boudreau, B. P. 1997. *Diagenetic Models and Their Implementation.* Springer-Verlag.

Bunde, T. A., G. E. Dearlove and S. H. Bishop. 1978. Aminoethylphosphonic acid-containing glycoproteins: The acid mucopolysaccharides-like components in mucus from *Metridium senile* (L.) *J. Exp. Biol.* 206(2): 215-221.

Burdige, D. J. 1991. The kinetics of organic matter remineralization in anoxic marine sediments. *J. Mar. Res.* 49: 727-761.

Cowie, G. L. and J. I. Hedges. 1992. Sources and reactivities of amino acids in coastal marine environments. *Limonl. Oceanogr.* 37(4): 703-724.

Cowie, G. L. and J. I. Hedges. 1994. Biochemical indicators of diagenetic alteration in natural organic matter mixtures. *Nature* 369: 304-307.

Cusson, M. and E. Bourget. 2005. Global patterns of macroinvertebrate production in marine benthic habitats. *Mar. Ecol. Prog. Ser.* 297: 1-14.

Eglinton, T. I. and D. J. Repeta. 2004. Organic Matter in the Contemporary Ocean *in* Treatise on Geochemistry, Chapter 6.06, pp. 145-180.

Enders, H. E. 1909. A study of the life history and habits of *Chaetopterus variopedatus*, Renier et Claparede. *J. Morph.* 20: 479-531.

Fanning, K. A. and M.E.Q. Pilson. 1973. Spectrophotometric determination of dissolved silica in natural waters. *Anal. Chem.* 45: 136–140.

Farrah, S. R. and G. W. Erdos. 1991. The production of antibacterial tubing, sutures and bandages by *in situ* precipitation of metallic salts. *Can. J. Microbiol.* 37: 445-449.

Fenchel, T. 1996. Worm burrows and oxic microniches in marine sediments. 1. Spatial and temporal scales. *Mar. Biol.* 127: 289-295.

Fleury, M. O. and D. V. Ashley. 1983. High-performance liquid chromatographic analysis of amino acids in physiological fluids: on-line precolumn derivatization with o-phthaldialdehyde. *Anal. Biochem.* 133(2): 330-335.

Frederiksen, M. S. and R. N. Glud. 2006. Oxygen dynamics in the rhizosphere of *Zostera marina*: A two-dimensional planar optode study. *Limnol. Oceanogr.* 51(2): 1072-1083.

Gaill, F. and S. Hunt. 1988. IV. Tubes. In: Westheidhe, W., Hermans, C. O. (Eds.), The ultrastructure of Polychaeta, Microfauna Marina, vol. 4. Stuttgard. Gustav Fischler Verlag, New York, pp. 61-70.

Gardiner, S. L. 1975. Errant polychaete annelids from North Carolina. *J. Elisha Mitchell Sci.* 91: 77-220.

Geraghty, M., J. F. Cronin, M. Devereux and M. McCann. 2000. Synthesis and antimicrobial activity of copper (II) and manganese (II) alpha, omega-dicarboxylate complexes. *Biometals* 13(1): 1-8.

Gerber, G. B., A. Léonard and P. Hantson. 2002. Carcinogenicity, mutagenicity and teratogenicity of manganese compounds. *Crit. Rev. Oncol. Hematol.* 42(1): 25-34.

Gillis, R. and R. J. Haro. 2010. Zoo Lab: A website for animal biology. http://bioweb.uwlax.edu/zoolab/index.htm

Goto, K., T. Komatsu and T. Furukawa. 1962. Rapid colorimetric determination of manganese in waters containing iron – a modification of formaldoxime method. *Anal. Chim. Acta* 27(4): 331-334.

Hall, P. O. J. and R. C. Aller. 1991. Rapid, small-volume flow injection analysis for$\sum CO_2$ and NH_4^+ in marine and freshwaters. *Limnol. Oceanogr.* 37(5): 1113-1119.

Hannides, A. K., S. M. Dunn and R. C. Aller. 2005. Diffusion of organic and inorganic solutes through macrofaunal mucus secretions and tube linings in marine sediments. *J. Mar. Res.* 63: 957-981.

Hargrave, B. T. 1972. Aerobic decomposition of sediment and detritus as a function of particle surface area and organic content. *Limnol. Oceanogr.* 17(4): 583-596.

Hedges, J. I. and R. G. Keil. 1995. Sedimentary organic matter preservation: an assessment and speculative synthesis. *Mar. Chem.* 49: 81-115.

Henrichs, S.M., J. W. Farrington, and C. Lee. 1984. Peru upwelling region sediments near 153S. 2. Dissolved free and total hydrolyzable amino acids. *Limnol. Oceanogr.* 29: 20-34.

Hymel, S. N. and C. J. Plante. 1998. Improved method of bacterial enumeration in in sandy and deposit-feeder gut sediments using the fluorescent stain 4,6-diamidino-2-phenylindole (DAPI). *Mar. Ecol. Prog. Ser.* 173: 299-304.

Ingalls, A.E., R. C. Aller, C. Lee and M. Y. Sun. 2000. The influence of deposit-feeding on chlorophyll-a degradation in coastal marine sediments. *J. Mar. Res.* 58: 631-651.

Jahauri, P. and J. N. Pattan. 2000. Ferromanganese nodules from the central Indian Ocean basin. In: Cronan D. S. (ed) Handbook of marine mineral deposits. CRC, Boca Raton, pp. 171-195

Jorgensen, B. B. 1978. A comparison of methods for the quantification of bacterial sulfate reduction in coastal marine sediments. 2. Calculations from mathematical models. *Geomicrobiol. J.* 1: 29-51.

Klimant, I., G. Holst and M. Kuhl. 1997. A simple fiberoptic sensor to detect the penetration of microsensors into sediments and other biogeochemical systems. *Limnol. Oceanogr.* 42(7): 1638-1643.

Kristensen, E., R. C. Aller and J. Y. Aller. 1991. Oxic and anoxic decomposition of tubes from the burrowing sea anemone *Ceriantheopsis americanus*: Implications for bulk sediment carbon and nitrogen balance. *J. Mar. Res.* 49: 589-617.

Kristensen, E. 2000. Organic matter diagenesis at the oxic/anoxic interface in coastal marine sediments, with emphasis on the role of burrowing animals. *Hydrobiol.* 426: 1-24.

Krom, M. D. and R. A. Berner. 1980. Adsorption of phosphate in anoxic marine sediments. *Limnol. Oceanogr.* 25(5): 797-806.

Lee, C. and C. Cronin. 1982. The vertical flux of particulate organic nitrogen in the sea: Decomposition of amino acids in the Peru upwelling area and the equatorial Atlantic. *J. Mar. Res.* 40: 227-251.

Lee, C, S. G. Wakeham, and J. I. Hedges. 2000. Composition and flux of particulate amino acids and chloropigments in equatorial Pacific seawater and sediments. *Deep-Sea Res. I* 47: 1535–1568.

Liu, Z. and C. Lee. 2007. The role of organic matter in the sorption capacity of marine sediments. *Mar. Chem.* 105: 240-257.

Mackin, J. E. and R. C. Aller. 1984. Ammonium adsorption in marine sediments. *Limnol. Oceanogr.* 29(2): 250-257.

Mandal, S., T. K. Karmakar, A. Ghosh, M. Fleck and D. Bandyopadhyay. 2011. Synthesis, crystal structure and antibacterial activity of a group of mononuclear manganese (II) Schiff base complexes. *Polyhedron* 30(5): 790-795.

Mangum, C. P., S. L. Santos and W. R. Rhodes, Jr. 1968. Distribution and feeding in the onuphid polychaete, *Diopatra cuprea* (Bosc). *Mar. Biol.* 2: 33-40.

Morse, J. W. and J. Morin. 2005. Ammonium interaction with coastal marine sediments: influence of redox conditions on K*. *Mar. Chem.* 95: 107-112.

Myers, A. C. 1972. Tube-worm-sediment relationships of *Diopatra cuprea* (Polychaeta: Onuphidae). *Mar. Biol.* 17:350-56.

Pettibone, M. H. 1963. Marine polychaete worms of the New England region, part 1. *U.S. Nat. Mus. Bull.* 227: 356 p.

Presley, B.J. 1971. Appendix: Techniques for Analyzing Interstitial Water Samples. Part I: Determination of Selected Minor and Major Inorganic Constituents *in* Winterer et al., 1971, Initial Reports of the Deep Sea Drilling Project, Volume VII, Washington, U.S. Government Printing Office, 1749-1755.

Redfield, A.C., B. H. Ketchum, and F. A. Richards, 1963. The influence of organisms on the composition of seawater. In: Hill, M.N., Editor, 1963. *The sea* Vol. 2, Interscience, New York, pp. 26–77.

Robertson, A. I. 1979. The relationship between annual production: biomass ratios and lifespans for marine microbenthos. *Oecologia (Berl.)* 38: 193-202.

Rosenfeld, J. K. 1979. Ammonium adsorption in nearshore anoxic sediments. *Limnol. Oceanogr*. 24: 356-364.

Ruttenberg, K. C. 1992. Development of a sequential extraction method for different forms of phosphorus in marine sediments. *Limnol. Oceanogr.* 37(7): 1460-1482.

Sewell, J. 2002. The Marine Biological Association. http://www.marlin.ac.uk

Soetaert, K., P. M. J. Herman and J. J. Middleburg. 1996. A model for early diagenetic processes from the shelf to abyssal depths. *Geochim. Cosmochim. Acta* 60: 1019-1040.

Solórzano, L. 1969. Determination of ammonia in natural waters by the phenolhypochlorite method. *Limnol. Oceanogr*. 14(5): 799-801.

Stevenson, F. J. 1962. Chemical state of nitrogen in rocks. *Geochim. Cosmochim. Acta* 26: 797-809.

Stewart, R. J., J. C. Weaver, D. E. Morse and J. H. Waite. 2004. The tube cement of *Phragmatopoma californica*: a solid foam. *J. Exp. Biol.* 207: 4727-4734.

Stewart, R. J. and C. S. Wang. 2010. Adaptation of Caddisfly larval silks to aquatic habitats by phosphorylation of H-fibroin serines. *Biomaromolecules* 11(4): 969-974.

Stookey, L. L. 1970. Ferrozine – A new spectrophotometric reagent for iron. *Anal Chem.* 42(7): 779-781.

Strickland, J. D. H. and T. R. Parsons. 1968. A practical handbook of seawater analysis. *Bull. Fisheries Res. Board Can.*, No. 167, 311 p.

Sun, C.J., G. E. Fantner, J. Adams, P. K. Hansma and J. H. Waite. 2007. The role of calcium and magnesium in the concrete tubes of the sandcastle worm. *J. Exp. Bilo.* 210: 1481-1488.

Sun, M. Y., R. C. Aller and C. Lee. 1991. Early diagenesis of chlorophyll-a in Long Island

Sound sediments: a measure of carbon flux and particle reworking. *J. Mar. Res.* 49: 379-401.

Tanur, A. E., N. Gunari, R. M. A. Sullan, C. J. Kavanagh and G. C. Walker. 2010. Insights into the composition, morphology, and formation of the calcareous shell of the serpulid *Hydroides dianthus*. *J. Struc. Biol.* 169: 145-160.

Thompson, M. L. and L. C. Schaffner. 2001. Population biology and secondary production of the suspension feeding polychaete *Chaetopterus* cf. *variopedatus*: Implications for benthic-pelagic coupling in lower Chesapeke Bay. *Limnol. Oceanogr.* 46(8): 1899-1907.

Tumbiolo, M. L. and J. A. Downing. 1994. An empirical model for the prediction of secondary production in marine benthic invertebrate populations. *Mar. Ecol. Prog. Ser.* 114: 165-174.

Turekian, K.K., and Wedepohl, K.H. 1961. Distribution of the elements in some major units of the Earth's crust: Geological Society of America Bulletin, v, 72, p. 175-191.

Ullman, W. J. and R. C. Aller. 1982. Diffusion coefficients in nearshore marine sediments. *Limnol. Oceanogr.* 27: 552-556.

Whelan, J.K. 1977. Amino acids in a surface sediment core of the Atlantic abyssal plain. *Geochim. Cosmochim. Acta* 41: 803-810.

Wilde, S. B. and C. J. Plante. 2002. Spatial heterogeneity of bacterial assemblages in marine sediments: The influence of deposit feeding by *Balanoglossus aurantiacus*. *Estuarine, Coastal & Shelf Science* 55: 97-107.

Wildish, D. J. and D. D. Kristmanson. 1997. Benthic suspension feeders and flow. Cambridge Univ. Press.

Zhang, F. S., C. Y. Lin, L. Z. Bian, G. P. Glasby and V. A. Zhamoida. 2002. Possible evidence for the biogenic formation of spheroidal ferromanganese concretions from the Eastern Gulf of Finland, the Baltic Sea. *Baltica* 15: 23-29.

Wang, X., H. C. Schröder, U. Schloßmacher and W. E. G. Müller. 2009. Organized bacterial assemblies in manganese nodules: evidence for a role of S-layers in metal deposition. *Geo-Mar. Lett.* 29:85-91.

Weiss, M. S., U. Abele, J. Weckesser, W. Welte, E. Schiltz and G. E. Schulz. 1991. Molecular architecture and electrostatic properties of a bacterial porin. *Science* 254: 1627-1630.

Appendix Table 1: Total Al, Fe, Mn and P in tube samples.

Tube Sample	time (days)	total Al (µg/g)	total Fe (µg/g)	total Mn (µg/g)	total P (µg/g)
t0	0	2939.3	34206.2	21205.2	906.1
			11402.1		
SdTUB	6.7	3301.3	39410.3	14368.4	996.0
	16.8	1750.6	32329.4	11296.4	1070.7
	27.8	2264.5	19263.6	15369.8	1152.8
	36.5	1546.2	16907.4	10312.8	1040.9
	50.8	3852.9	14597.5	13534.9	1260.5
	64.6	1389.4	14685.3	11919.1	1141.8
	76.4	2395.8	11695.9	13690.6	1149.8
	85.2	2407.4	12293.3	13986.6	1240.1
	95.3	2337.0	9749.8	10178.9	909.5
	111.2	1844.9	18819.1	10647.9	1191.4
	127.2	1740.8	19180.9	6143.0	1203.7
PcTUB	6.7	1774.6	28317.3	12977.4	1161.9
	16.8	2575.5	39198.9	12595.0	1022.2
	27.8	2259.2	16958.8	14626.1	1203.9
	36.5	2491.6	14043.5	10837.3	1141.4
	50.8	2206.8	18042.0	9248.4	1233.6
	64.6	2427.8	15276.0	10040.2	1166.4
	76.4	1840.3	15215.5	8317.3	1038.8
	85.2	3760.5	19317.2	7357.3	1077.0
	95.3	2254.2	18046.1	6408.1	911.5
	111.2	2674.5	19941.2	10176.4	1201.0
	127.2	2226.7	14078.5	9051.2	1074.4
LchTUB	6.0	2500.5	20703.4	8564.7	1066.5
	16.0	1512.9	17514.0	8246.1	1010.8
	27.0	2419.5	22404.2	6909.8	1054.6
	35.7	2590.6	14078.3	7608.9	1033.2
	50.0	1919.1	16053.4	6579.6	1072.5
	63.9	2705.5	18278.8	3221.2	656.1
	75.6	2522.7	20062.4	4678.9	982.4
	84.4	1206.2	15897.1	5767.9	1068.4
	94.5	2122.4	21021.3	5226.0	1203.9
	110.4	1946.0	27474.5	6647.0	1291.4

126.4	2647.2	24337.3	3404.3	796.1

Appendix Table 2: Total Al, Fe, Mn and P in sediment samples.

Sediment sample	time (days)	total Al (µg/g)	total Fe (µg/g)	total Mn (µg/g)	total P (µmoles/g)	inorganic P (µmoles/g)
t0	0	10662.9	13972.2	464.7	46.97	22.61
SdTUB	6.7	9760.5	14016.3	509.7	35.71	13.98
	16.8	13124.7	15460.0	455.3	39.09	13.70
	27.8	11095.9	13933.3	461.5	36.36	14.55
	36.5	11083.7	12211.5	425.5	37.01	15.96
	50.8	8795.0	14088.1	458.4	40.66	15.87
	64.6	12970.7	14903.5	523.9	41.57	17.79
	76.4	14098.3	16823.3	817.8	38.16	15.68
	85.2	15032.7	18689.8	777.9	40.78	13.70
	95.3	12101.9	14966.4	551.0	32.70	14.79
	111.2	10431.7	13292.5	530.9	33.21	15.09
	127.2	11291.9	14891.5	510.1	42.03	19.55
PcTUB	6.7	8695.7	12901.8	428.5	36.75	16.88
	16.8	10222.7	12791.0	435.1	34.28	14.76
	27.8	10862.4	12778.7	577.6	30.46	11.42
	36.5	11923.0	15288.9	572.2	37.21	15.68
	50.8	12166.3	15485.5	459.7	39.17	18.09
	64.6	12907.4	15945.5	517.5	35.94	18.66
	76.4	11915.7	15209.4	430.8	41.69	19.15
	85.2	10945.3	14269.8	532.8	36.32	17.09
	95.3	12831.7	16874.7	418.9	36.83	16.28
	111.2	11014.9	13958.5	546.6	31.75	15.06
	127.2	10339.9	17809.1	740.8	51.83	18.22
LchTUB	6.0	9085.1	13728.3	409.9	39.11	15.67
	16.0	9594.2	13083.9	400.4	31.07	12.03
	27.0	12270.5	15858.6	386.8	33.15	10.21
	35.7	10972.3	14287.4	430.8	30.12	15.36
	50.0	8325.4	13207.8	362.0	37.01	14.45
	63.9	11765.0	14437.6	452.0	34.55	16.27
	75.6	9522.7	13324.9	427.5	33.41	15.68
	84.4	7811.5	14472.2	425.2	38.04	15.11
	94.5	11310.4	14753.0	433.0	36.18	18.07

	110.4	10261.5	13840.7	379.1	38.42	18.68
	126.4	10238.1	12951.8	441.1	31.60	20.09
Control	6.7	8839.3	14793.5	525.4	41.01	16.51
	16.8	10615.0	13130.0	384.5	39.75	17.66
	27.8	11803.0	12024.9	412.7	29.73	10.42
	36.5	11755.1	13603.9	372.9	32.89	10.85
	50.8	8404.3	11281.7	421.8	38.32	18.43
	64.6	11737.0	15312.0	500.4	39.84	17.09
	76.4	10734.2	14245.4	461.7	41.60	18.84
	85.2	11944.0	14999.3	459.9	39.71	16.95
	95.3	11432.2	13713.3	409.1	35.63	14.55
	111.2	12336.8	15347.9	598.0	36.99	16.19
	127.2	14621.5	16168.3	484.9	39.36	17.77